Boundary-layer receptivity to external disturbances using multiple scales

Simone Zuccher · Paolo Luchini

Abstract Non-homogeneous multiple scales are introduced to solve the resonant problem of non-parallel boundary-layer receptivity originating from the quadratic mixing of environmental disturbances. The resulting algorithm is computationally inexpensive and can be efficiently included in industrial codes for transition prediction. The mutual interactions between acoustic wave, vorticity wave, wall vibration and wall roughness are discussed in detail and the receptivity coefficient, which relates the amplitude of the excited wave to the amplitude of the exciting sources, is computed. The largest effect is found for the interaction between acoustic waves and wall roughness perturbations. Other coupling mechanisms are less effective. By comparing parallel and non-parallel results, it is found that flow non-parallelism can play a non-negligible role even in Blasius' boundary layer, although the largest effects are evident for the three-dimensional boundary layer over an infinite swept wing. For the particular case of wall roughness—wall vibration mixing, the velocity disturbance is shown to be exactly equal to the velocity perturbation induced by wall roughness alone on a wall vibrating in the normal direction.

1 Introduction to the problem of receptivity

Within the scope of boundary-layer stability analysis, receptivity [49, 52] has been receiving large attention in the last decades owing to its potential to improve transition-prediction criteria by including the response to external disturbances. The classical e^N method, still employed for airplane design, is based on the ansatz that transition occurs when the total amplification of the leading instability mode (obtained as the solution to a homogeneous problem) attains a given value. This is only a realistic assumption for practical situations where both the transition threshold and the amplitude of external sources of excitation exhibit little variation from one case to another. Here, instead, we focus on the relationship between the amplitude of the Tollmien-Schlichting instability wave (TS wave) generated inside the boundary layer and the physical amplitude of the environmental disturbances that cause it.

Typical external disturbances are acoustic waves, freestream vorticity waves and wall vibrations. Even when their frequency is close to that of TS waves,

S. Zuccher (✉)
Department of Computer Science, Università di Verona,
37134 Verona, Italy
e-mail: simone.zuccher@univr.it

P. Luchini
Department of Industrial Engineering,
Università di Salerno, 84084 Fisciano, SA, Italy
e-mail: luchini@unisa.it

these disturbances cannot resonate with TS waves because their wavelength is much larger.[1] On the other hand, resonance can be achieved if some wavelength conversion mechanism ensures the adaptation of the exciting wavelength [30, 31, 53]. This wavelength-conversion effect can be provided by the rapid growth of the boundary layer near the leading edge or by a rapid variation of the wall boundary conditions that induce a fast adaptation of the boundary layer. Consequently, the wide range of receptivity configurations analyzed in published works (see Ref. [33] for a review on the progresses made in the 1980s and Ref. [57] for a later review summarizing theoretical modeling, numerical simulations, and experiments) can ultimately be grouped as (a) leading-edge receptivity, (b) sudden boundary-layer forced adjustment receptivity and (c) *distributed* (surface roughness) receptivity. Here we are only interested in problem (c).

Receptivity mechanisms can also be organized according to where the unsteadiness originates from, i.e. receptivity to freestream disturbances (acoustic and vorticity waves) or receptivity to disturbances at the wall (wall vibration).

Among the first class of mechanisms, localized receptivity to acoustic waves interacting with wall roughness has been the most studied. Notable experimental contributions are those by Kachanov [39] and Saric *et al.* [55], while the theoretical problem was first approached by Goldstein [31], Ruban [53] and Zhigulev & Fedorov [68]. Within the triple-deck theory, small roughness heights led to a linearized formulation [31, 32], which was later numerically extended to deal with larger heights that require the nonlinear approach for both two-dimensional [8] and three-dimensional [61] roughness elements. After the first asymptotic theories, receptivity to acoustic waves was tackled by solving an inhomogeneous OS problem in the Fourier transform space and by determining the amplitude of the instability wave as the residue of the pole that corresponds to the TS eigenmode of the OS equation. This OS approach was first applied in the linear case (small heights) [17, 19] and later in the non-linear one (large heights) [50]. In the study of

receptivity to acoustic waves, other "tuning" mechanisms were considered such as suction and blowing [7, 16, 24], rapid static pressure variations or marginally separated flows [33, 34], and the descending step [2]. Also the non localized receptivity to acoustic waves has been investigated [14, 20, 21]. The problem of receptivity to vorticity waves, on the other hand, was studied in both localized [15, 26, 41, 42] and non localized frameworks [23], and by considering the mutual interaction with acoustic waves without resorting to a local non-homogeneity of the mean flow [65]. Significant and original experimental data on vortical receptivity can be found in Ref. [25], which is also a good review paper with further references. More recent theoretical results on local and distributed receptivity to both acoustic and vortical disturbances were obtained by Wu [66, 67], who compared them with the experiments of Dietz [25] finding a good agreement.

Historically, the other class of mechanisms (unsteady disturbances generated at the wall) was the first problem considered. The typical configuration is the vibrating ribbon, which was experimentally investigated by Schubauer and Skramstad [59] and then theoretically, almost 20 years later, by Gaster [27]. The first theoretical studies of boundary-layer receptivity to wall vibration were carried by Terent'ev [54, 62, 63]; later on the problem of the vibrating ribbon was revisited [3, 29, 60] and extended to the study of instability waves in wall boundary layers excited by various types of Dirac sources [46–48]. More recently the receptivity to distributed wall vibrations has been considered [40].

As far as it is known to the authors, the receptivity to structural vibration is restricted to the works of Chiu *et al.* [13] and Chiu and Norton [12], who considered the receptivity to transverse structural vibration on the leading edge.

References to three-dimensional base flows and swept-wing boundary layers can be found in Ref. [38].

2 Multiple scales among possible modeling approaches

Boundary-layer receptivity has been analyzed using several different theoretical approaches, such as asymptotic expansions based on large Reynolds numbers, Orr-Sommerfeld (OS) formulations, parabolized stability equation (PSE) and direct numerical simulation (DNS). All these techniques can be coupled with

---

[1]This is because the phase speed of TS waves turns out to be a fraction of the freestream velocity, whereas the phase speed of vorticity waves is precisely the freestream velocity and the phase speed of sound waves is even larger until the flow remains subsonic.

an adjoint formulation, to obtain the sensitivity of the TS waves to modifications of the base flow or boundary condition [1, 35, 36, 44, 51].

Triple-deck modeling was, historically, the first approach to receptivity [30, 31, 33, 34, 53]. The solution is expanded as the sum of a steady base flow, a steady perturbation due to wall roughness, and an unsteady perturbation due to the unsteady source (e.g. acoustic wave). An analytical expression for the receptivity coefficient was found in the linear case [31], while for larger roughness heights the problem was solved numerically [8, 61]. The main disadvantage of this class of asymptotic methods, however, is that they work well only for very large Reynolds numbers, in the vicinity of the lower branch of the neutral-stability curve, and for specific dimensions of the hump that are on a scale specified in the formulation.

The OS approach, on the contrary, is valid for finite Reynolds numbers, both near and away from branch I, and allows the study of frequency effects at different Reynolds numbers [17, 19]. The solution is the sum of the Blasius boundary layer $v_0(y)$, independent of x, an unsteady flow $v_\epsilon(x, y, t)$ due to the interaction between the boundary layer and the unsteady source (Stokes flow), a steady flow $v_\delta(x, y)$ due to the interaction between the wall disturbance and the boundary layer, and an unsteady flow $v_{\epsilon\delta}(x, y, t)$ due to the interaction of the previous ones. The latter is the resonant wave. Boundary conditions are moved from $y = \delta h(x)$ (wall shape) to $y = 0$ using a Taylor expansion. The original assumption of small hump heights can be overcome by using an interacting boundary layer model [50] and the parallel-flow limitation relaxed by introducing a Taylor expansion of the laminar mean-flow profile at the location of the roughness and employing a Fourier transform approach [5].

PSE can incorporate non-homogeneous initial and boundary conditions, with the advantage of a modest computational effort compared to the solution of the Navier-Stokes equations. For this reason they have been applied to receptivity studies and transition prediction, accounting also for non-parallel effects [1, 6, 35, 51]. Unfortunately, depending on the way the equations are implemented in a code, numerical stability problems can arise with diminishing x-step, so that formally the method does not even converge unless ad-hoc stabilization techniques are added.

DNS does not assume any modeling and solves directly the unsteady Navier-Stokes equations at the expense of a heavy computational effort. The sensitivity of the TS waves to the hump height and length, and to the acoustic frequency, was computed [10, 11] and verified against the linear approach [31] and available experimental data [43, 55].

The technique we shall concentrate upon here is the multiple-scale method [9, 28]. This is a classical asymptotic approximation which is applied in physics every time a problem, whose oscillating solution is known for constant parameters, is to be solved with those constants being replaced by slowly varying functions [4, 64]. The condition for applying this method is the existence of two separated scales of temporal or spatial variation. This is typically the case of TS waves, where variations of the base flow are quite slow in the streamwise direction as compared to the TS wavelength.

If the base flow were streamwise-constant (parallel flow), the fast-varying perturbation would be described by a complex exponential. In the general case, the solution $y(x)$ is assumed to be of the form $A(x, \tilde{\epsilon})e^{\phi(x)/\tilde{\epsilon}}$, where $\tilde{\epsilon}$ is a small parameter accounting for the scale ratio. Function $A(x, \tilde{\epsilon})$, the slowly varying (generally complex) amplitude, is expanded in a power series of the small parameter $\tilde{\epsilon}$; a corresponding expansion of the governing equations leads to a hierarchy of problems at different orders with respect to $\tilde{\epsilon}$.

In Appendix A, the homogeneous version of multiple scales, also known as WKB approximation (after Wentzel, Kramers and Brillouin), is reported for reference.

In fluid dynamics the leading order of the multiple-scale expansion, as developed by [9, 28], is generally referred to as the "parallel" (or sometimes "quasi-parallel") approximation, whereas the subsequent term of the expansion is the "non-parallel correction". The homogeneous multiple-scale technique was applied to account for non-parallel effects in the study of the stability of a two-dimensional incompressible boundary layer in [56], and more recently to analyse the stability of three-dimensional incompressible boundary layers in [45]. In the theory of receptivity, multiple scales were pioneered in Russia by Zhigulev, Tumin, Fedorov and their colleagues, leading to a series of journal papers summarized in the monograph by Zhigulev and Tumin [69].

As compared to the other approaches previously described, multiple scales can be preferable for the study of boundary-layer receptivity because of different reasons. First, they allow us to naturally include
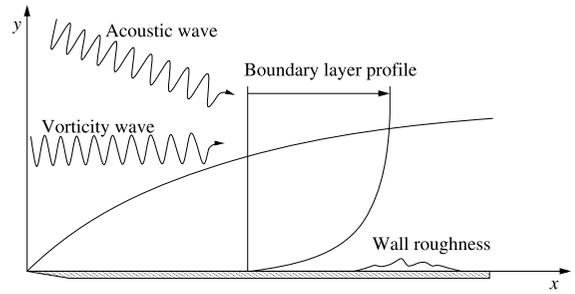
non-parallel effects due to boundary-layer growth, which may be important in some applications (e.g. accelerating or decelerating boundary layers or the boundary layer on a swept wing). Second, they yield reasonably accurate results at moderately high Reynolds number, in contrast with other asymptotic methods (e.g. triple deck) that only converge at impractically large Reynolds numbers where the flow in reality is already turbulent. Finally, multiple-scale approximations provide computationally inexpensive numerical codes without the numerical-stability problems that plague PSE.

The work presented here was carried out a few years ago [70] to treat the receptivity problem in boundary layers by developing a *non-homogeneous* version of multiple scales in the amplification region, where the boundary-layer grows slowly. The method is used to analyse interactions between (i) acoustic waves and wall roughness, (ii) vorticity waves and wall roughness, and (iii) acoustic and vorticity waves. The coupling between (iv) wall vibration and wall roughness, which is a very common condition for an airplane wing or for the blade of a turbo-machine, is analyzed in Appendix C. Even though multiple scales have been used and compared with other approaches (for instance at CIRA, the Italian Aerospace Research Center), their systematic description for the study of receptivity and their suitability for industry applications have not received much attention. For this reason their application to a non homogeneous, resonant problem is here reported in detail (see, in particular, Sects. 4 and 5).

3 Problem formulation and linearization

The problem is governed by the dimensionless, incompressible Navier-Stokes equations:

$$\hat{u}_{\hat{x}} + \hat{v}_{\hat{y}} + \hat{w}_{\hat{z}} = 0$$

$$\hat{u}_{\hat{t}} + \hat{u}\hat{u}_{\hat{x}} + \hat{v}\hat{u}_{\hat{y}} + \hat{w}\hat{u}_{\hat{z}}$$
$$= -\hat{p}_{\hat{x}} + \frac{\hat{u}_{\hat{x}\hat{x}} + \hat{u}_{\hat{y}\hat{y}} + \hat{u}_{\hat{z}\hat{z}}}{R}$$

$$\hat{v}_{\hat{t}} + \hat{u}\hat{v}_{\hat{x}} + \hat{v}\hat{v}_{\hat{y}} + \hat{w}\hat{v}_{\hat{z}} \qquad (1)$$
$$= -\hat{p}_{\hat{y}} + \frac{\hat{v}_{\hat{x}\hat{x}} + \hat{v}_{\hat{y}\hat{y}} + \hat{v}_{\hat{z}\hat{z}}}{R}$$

$$\hat{w}_{\hat{t}} + \hat{u}\hat{w}_{\hat{x}} + \hat{v}\hat{w}_{\hat{y}} + \hat{w}\hat{w}_{\hat{z}}$$

Fig. 1 Possible external disturbances inducing transition to turbulence in the boundary layer over a flat plate

$$= -\hat{p}_{\hat{z}} + \frac{\hat{w}_{\hat{x}\hat{x}} + \hat{w}_{\hat{y}\hat{y}} + \hat{w}_{\hat{z}\hat{z}}}{R},$$

together with the relevant initial and boundary conditions. Velocities are normalized with the outer velocity U_∞^* (a star $\cdot^*$ denoting dimensional quantities, a hat $\hat{\cdot}$ dimensionless ones), whereas the streamwise, wall-normal and spanwise coordinates x, y and z are scaled with a typical boundary-layer thickness $\delta_0^* = \sqrt{x_I^* \nu^*/U_\infty^*}$ (x_I^* being the first neutral point of the neutral curve), and time with δ_0^*/U_∞^*. The Reynolds number is defined as $R = \delta_0^* U_\infty^*/\nu^* = \sqrt{x_I^* U_\infty^*/\nu^*} = \sqrt{Re_{x_I^*}}$.

Referring to Fig. 1, we consider a general steady, incompressible boundary layer past a flat plate. Some disturbances can originate in the external flow (acoustic and vorticity waves), others at the wall (wall vibration and wall roughness). Following what was already done by others [17, 19], we introduce two small disturbances $\epsilon \hat{\mathbf{v}}_\epsilon(\hat{x}, \hat{y}, \hat{z}) e^{-i\hat{\omega}_\epsilon \hat{t}}$ and $\delta \hat{\mathbf{v}}_\delta(\hat{x}, \hat{y}, \hat{z}) e^{-i\hat{\omega}_\delta \hat{t}}$, where $\hat{\mathbf{v}}_\epsilon = (u_\epsilon, v_\epsilon, w_\epsilon)$ and $\hat{\mathbf{v}}_\delta = (u_\delta, v_\delta, w_\delta)$ are respectively an unsteady wave of amplitude ϵ generated by a general unsteady excitation source behaving as $e^{-i\hat{\omega}_\epsilon \hat{t}}$, and an unsteady wave of amplitude δ due to another general unsteady excitation source behaving as $e^{-i\hat{\omega}_\delta \hat{t}}$. These two perturbations are superimposed to a steady base flow $\hat{\mathbf{V}}(\hat{x}, \hat{y}, \hat{z})$. Their interaction generates beat waves, respectively

$$\epsilon\delta \hat{\mathbf{v}}_{\epsilon\delta}^+(\hat{x}, \hat{y}, \hat{z}) e^{-i(\hat{\omega}_\epsilon + \hat{\omega}_\delta)\hat{t}} \quad \text{and}$$

$$\epsilon\delta \hat{\mathbf{v}}_{\epsilon\delta}^-(\hat{x}, \hat{y}, \hat{z}) e^{-i(\hat{\omega}_\epsilon - \hat{\omega}_\delta)\hat{t}}$$

at order $\epsilon\delta$, plus other waves at higher orders. The wavelength and frequency of the waves at orders ϵ and δ, in general, are different from those typical of TS waves. Their interaction at order $\epsilon\delta$, however,

could generate a resonant wave. If we assume that the latter is $\epsilon\delta\hat{\mathbf{v}}_{\epsilon\delta}^+(\hat{x}, \hat{y}, \hat{z})\mathrm{e}^{-i(\hat{\omega}_\epsilon+\hat{\omega}_\delta)\hat{t}}$, allowing one of the interacting frequencies to be negative, then its amplitude is much larger than the amplitude of $\epsilon\delta\hat{\mathbf{v}}_{\epsilon\delta}^-(\hat{x}, \hat{y}, \hat{z})\mathrm{e}^{-i(\hat{\omega}_\epsilon-\hat{\omega}_\delta)\hat{t}}$, which can be neglected. The velocity field inside the boundary layer $\hat{\mathbf{v}}(\hat{x}, \hat{y}, \hat{z}, \hat{t})$ is thus decomposed into different contributions originating from the steady base flow ($\hat{\mathbf{V}}$), from different environmental sources ($\hat{\mathbf{v}}_\epsilon$ and $\hat{\mathbf{v}}_\delta$) and from their mutual interaction ($\hat{\mathbf{v}}_{\epsilon\delta}$),

$$
\begin{aligned}
\hat{\mathbf{v}}(\hat{x}, \hat{y}, \hat{z}, \hat{t}) = {} & \hat{\mathbf{V}}(\hat{x}, \hat{y}, \hat{z}) + \epsilon\hat{\mathbf{v}}_\epsilon(\hat{x}, \hat{y}, \hat{z})\mathrm{e}^{-i\hat{\omega}_\epsilon\hat{t}} \\
& + \delta\hat{\mathbf{v}}_\delta(\hat{x}, \hat{y}, \hat{z})\mathrm{e}^{-i\hat{\omega}_\delta\hat{t}} \\
& + \epsilon\delta\hat{\mathbf{v}}_{\epsilon\delta}(\hat{x}, \hat{y}, \hat{z})\mathrm{e}^{-i(\hat{\omega}_\epsilon+\hat{\omega}_\delta)\hat{t}} \\
& + \mathcal{O}(\epsilon^2) + \mathcal{O}(\delta^2) + \cdots,
\end{aligned} \tag{2}
$$

where $\hat{\mathbf{v}}_{\epsilon\delta}$ is understood as $\hat{\mathbf{v}}_{\epsilon\delta}^+$. Of course, as a particular case one of the two frequencies might be zero.

If the velocity decomposition (2) is substituted in the Navier-Stokes equations (1), and the latter are suitably expanded, one finds three linear problems at orders ϵ, δ and $\epsilon\delta$.

Linearization can also be applied to the boundary conditions at the wall. In the case of wall roughness, the wall shape is expressed as $\delta h(\hat{x})$, where δ is the typical wall-roughness scale and $h(\hat{x})$ is an order-one function of the streamwise coordinate. This disturbance is stationary, and thus $\hat{\omega}_\delta = 0$.

On the other hand, wall vibration can generate an unsteady motion of the wall in the streamwise, spanwise or wall-normal direction. In the first two cases the problem reduces to the well-known flow near an oscillating flat plate (Stokes's second problem [58]), while in the second one the position of the wall as a function of time can be described by $\epsilon\mathrm{e}^{-i\hat{\omega}_\epsilon\hat{t}}$ where ϵ is the typical amplitude of the vibration with a characteristic frequency $\hat{\omega}_\epsilon$. If both disturbances (wall roughness and wall vibration) are acting at the wall, the wall shape must be described by the function $H(\hat{x}, \hat{t}) = \delta h(\hat{x}) + \epsilon\mathrm{e}^{-i\hat{\omega}_\epsilon\hat{t}}$.

In Appendix C we prove that wall vibration coupled with wall roughness does not lead to resonance. This allows us to consider the effect of wall roughness alone, which reduces the wall shape $H(\hat{x}, \hat{t})$ to the steady form $H(\hat{x}) = \delta h(\hat{x})$.

Boundary conditions defined at $\hat{y} = \delta h(\hat{x})$ can be shifted to $\hat{y} = 0$ via linearization because δ is a small

parameter. The Taylor expansion of the velocity field $\hat{\mathbf{v}}$ about the position $\hat{y} = 0$ leads to

$$
\begin{aligned}
\hat{\mathbf{v}}(\hat{x}, \hat{y}, \hat{z}, \hat{t}) = {} & \hat{\mathbf{v}}(\hat{x}, 0, \hat{z}, \hat{t}) + \delta h(\hat{x})\frac{\partial\hat{\mathbf{v}}(\hat{x}, \hat{y}, \hat{z}, \hat{t})}{\partial\hat{y}}\bigg|_{\hat{y}=0} \\
& + \frac{1}{2}\delta^2 h^2(\hat{x})\frac{\partial^2\hat{\mathbf{v}}(\hat{x}, \hat{y}, \hat{z}, \hat{t})}{\partial\hat{y}^2}\bigg|_{\hat{y}=0} \\
& + \mathcal{O}(\delta^3) = \mathbf{0}.
\end{aligned} \tag{3}
$$

When the expansion (2) is introduced in the linearization (3), non-homogeneous boundary conditions originate at order δ and $\epsilon\delta$,

$$
\begin{aligned}
& \hat{\mathbf{V}}(\hat{x}, 0, \hat{z}) = 0 \\
& \hat{\mathbf{v}}_\epsilon(\hat{x}, 0, \hat{z}) = 0 \\
& \hat{\mathbf{v}}_\delta(\hat{x}, 0, \hat{z}) = -h(\hat{x})\frac{\partial\hat{\mathbf{V}}(\hat{x}, \hat{y}, \hat{z})}{\partial y}\bigg|_{\hat{y}=0} \\
& \hat{\mathbf{v}}_{\epsilon\delta}(\hat{x}, 0, \hat{z}) = -h(\hat{x})\frac{\partial\hat{\mathbf{v}}_\epsilon(\hat{x}, \hat{y}, \hat{z})}{\partial\hat{y}}\bigg|_{\hat{y}=0}.
\end{aligned} \tag{4}
$$

The system of linearized Navier-Stokes equations and boundary conditions at the wall can now be formally and compactly written as

$$
\boldsymbol{L}_\epsilon(\hat{\mathbf{V}}, R)\hat{\mathbf{f}}_\epsilon = \hat{\mathbf{y}}_\epsilon \tag{5}
$$

$$
\boldsymbol{L}_\delta(\hat{\mathbf{V}}, R)\hat{\mathbf{f}}_\delta = \hat{\mathbf{y}}_\delta \tag{6}
$$

$$
\boldsymbol{L}_{\epsilon\delta}(\hat{\mathbf{V}}, R)\hat{\mathbf{f}}_{\epsilon\delta} = \hat{\mathbf{y}}_{\epsilon\delta}. \tag{7}
$$

Here $\hat{\mathbf{f}}_\gamma = (\hat{u}_\gamma, \hat{v}_\gamma, \hat{w}_\gamma, \hat{p}_\gamma)$, with $\gamma \in \{\epsilon, \delta, \epsilon\delta\}$, is the vector of unknowns while $\boldsymbol{L}_\gamma(\hat{\mathbf{V}}, R)$ is a linear operator that depends on the base flow

$$
\hat{\mathbf{V}} = \big(\hat{U}(\hat{x}, \hat{y}, \hat{z}), \hat{V}(\hat{x}, \hat{y}, \hat{z}), \hat{W}(\hat{x}, \hat{y}, \hat{z})\big)
$$

and Reynolds number R. The right-hand-side (RHS) terms $\hat{\mathbf{y}}_\gamma$ ($\gamma \in \{\epsilon, \delta, \epsilon\delta\}$) at orders ϵ and δ originate from the possible non homogeneous boundary conditions at the wall or at infinity (see conditions (4) at the wall). At order $\epsilon\delta$, on the other hand, not only boundary conditions contribute to the RHS but also the coupling terms coming from the nonlinear part of the original Navier-Stokes equations, i.e. $\hat{\mathbf{y}}_{\epsilon\delta} = -[0, a, b, c]^T$,

with

$$a = \hat{u}_\epsilon (\hat{u}_\delta)_x + \hat{u}_\delta (\hat{u}_\epsilon)_x + \hat{v}_\epsilon (\hat{u}_\delta)_y$$
$$+ \hat{v}_\delta (\hat{u}_\epsilon)_y + \hat{w}_\epsilon (\hat{u}_\delta)_z + \hat{w}_\delta (\hat{u}_\epsilon)_z$$
$$b = \hat{u}_\epsilon (\hat{v}_\delta)_x + \hat{u}_\delta (\hat{v}_\epsilon)_x + \hat{v}_\epsilon (\hat{v}_\delta)_y$$
$$+ \hat{v}_\delta (\hat{v}_\epsilon)_y + \hat{w}_\epsilon (\hat{v}_\delta)_z + \hat{w}_\delta (\hat{v}_\epsilon)_z \qquad (8)$$
$$c = \hat{u}_\epsilon (\hat{w}_\delta)_x + \hat{u}_\delta (\hat{w}_\epsilon)_x + \hat{v}_\epsilon (\hat{w}_\delta)_y$$
$$+ \hat{v}_\delta (\hat{w}_\epsilon)_y + \hat{w}_\epsilon (\hat{w}_\delta)_z + \hat{w}_\delta (\hat{w}_\epsilon)_z.$$

It should be noticed that equation (7) has to be satisfied under resonant conditions and thus requires additional care.

4 Non-homogeneous multiple-scale theory applied to a one-dimensional resonant problem

In order to explain the use of multiple scales for the non homogeneous and resonant problem (7), let us focus on a simple time-dependent (one-dimensional) system.

As known from the study of the harmonic oscillator driven by a sinusoidal forcing, $\ddot{x} + \omega_0^2 x = F_0 \cos \omega t$, in the limit $\omega \to \omega_0$, i.e. under resonant conditions, the particular solution $x_p(t)$, induced by the non-homogeneous source, can be rewritten as $F_0 t \sin(\omega_0 t)/(2\omega_0)$. This expression emphasizes the presence, in the case of undamped oscillations, of a secular term that grows indefinitely (and linearly) with time for $t \to \infty$.

On the other hand, if an oscillator (or another model of a physical phenomenon) shows a separation of scales, for instance in time, multiple scales can efficiently account for it through the introduction of a small parameter $\tilde{\epsilon}$ that leads to the definition of a new "slow" variable $T = \tilde{\epsilon} t$ (see Appendix A for a simple, one-dimensional and homogeneous formulation). When multiple scales are employed for the study of resonant problems, the presence of the secular term proportional to t leads to a solution that behaves as $T/\tilde{\epsilon}$ and still grows in time, but that provides an $\mathcal{O}(1/\tilde{\epsilon})$ effect. Two choices are available for introducing the resonant forcing at the correct order in $\tilde{\epsilon}$. If the fundamental order in the multiple-scale expansion is $1/\tilde{\epsilon}$, then the resonant forcing should be introduced at order $\tilde{\epsilon}^0$; if the leading order is $\tilde{\epsilon}^0$, as in the multiple-scale theory here presented, then the forcing term must

be multiplied by $\tilde{\epsilon}^1$. Under these assumptions, a time-dependent linear system forced to resonant conditions reads

$$\boldsymbol{H}(t)\frac{d\mathbf{x}(t)}{dt} + \boldsymbol{A}(t)\mathbf{x}(t) = \tilde{\epsilon}\mathbf{y}(t), \qquad (9)$$

where matrices $\boldsymbol{H}$ and $\boldsymbol{A}$ are slowly varying with time t, $\mathbf{x}$ is the state vector, $\tilde{\epsilon}$ is, as noticed, the small parameter that accounts for the slow variation with respect to t, and $\mathbf{y}$ is the resonant forcing term, appearing at order $\tilde{\epsilon}$ for the reason explained above.

The solution $\mathbf{x}$ is assumed to be representable in the form

$$\mathbf{x}(t) = \mathbf{f}(T)\exp\big(\phi(T)/\tilde{\epsilon}\big)$$
$$= \big(\mathbf{f}_0(T) + \tilde{\epsilon}\mathbf{f}_1(T) + \tilde{\epsilon}^2\mathbf{f}_2(T) + \cdots\big)$$
$$\times \exp\big(\phi(T)/\tilde{\epsilon}\big),$$

where the exponential is a fast varying oscillating function, while vector $\mathbf{f}(T)$ is the slowly varying part and is expanded in series of the small parameter $\tilde{\epsilon}$. Under resonant conditions, on the other hand, the forcing $\mathbf{y}(t)$ is also fast varying, and can be expressed as

$$\mathbf{y}(t) = \big(\mathbf{y}_0(T) + \tilde{\epsilon}\mathbf{y}_1(T) + \tilde{\epsilon}^2\mathbf{y}_2(T) + \cdots\big)$$
$$\times \exp\big(\psi(T)/\tilde{\epsilon}\big).$$

After expressing the derivative with respect to t in terms of T (see Appendix A) and introducing it in the original system (9), by separating the contributions at different orders with respect to $\tilde{\epsilon}$ the following hierarchy of linear systems is obtained,

$$\tilde{\epsilon}^0\bigg(\frac{d\phi}{dT}\boldsymbol{H}(T)\mathbf{f}_0(T) + \boldsymbol{A}(T)\mathbf{f}_0(T)\bigg)e^{\frac{\phi(T)}{\tilde{\epsilon}}} = 0$$

$$\tilde{\epsilon}\bigg(\frac{d\phi}{dT}\boldsymbol{H}(T)\mathbf{f}_1(T) + \frac{d\mathbf{f}_0}{dT} + \boldsymbol{A}(T)\mathbf{f}_1(T)\bigg)e^{\frac{\phi(T)}{\tilde{\epsilon}}}$$
$$= \tilde{\epsilon}\mathbf{y}_0(T)e^{\frac{\psi(T)}{\tilde{\epsilon}}} \qquad (10)$$

$$\vdots = \vdots$$

$$\tilde{\epsilon}^n\bigg(\frac{d\phi}{dT}\boldsymbol{H}(T)\mathbf{f}_n(T) + \frac{d\mathbf{f}_{n-1}}{dT} + \boldsymbol{A}(T)\mathbf{f}_n\bigg)e^{\frac{\phi(T)}{\tilde{\epsilon}}}$$
$$= \tilde{\epsilon}^n\mathbf{y}_{n-1}(T)e^{\frac{\psi(T)}{\tilde{\epsilon}}}.$$

The homogeneous system at order zero ($\tilde{\epsilon}^0$) is a generalized eigenvalue problem

$$\big[\boldsymbol{A}(T) + \lambda_k(T)\boldsymbol{H}(T)\big]\mathbf{u}_k(T) = 0 \qquad (11)$$

where $\lambda_k(T) = \phi'(T)$ is the eigenvalue and $\mathbf{u}_k(T) = \mathbf{f}_0(T)$ is the right eigenvector. The latter is not unique, i.e. $\mathbf{f}_0(T) = \mathbf{u}_k(T) = c_k(T)\tilde{\mathbf{u}}_k(T)$, where $c_k(T)$ is a multiplicative function and $\tilde{\mathbf{u}}_k(T)$ is the right eigenvector arbitrarily normalized.

At any other order, terms proportional to $\mathrm{e}^{\frac{\psi(T)-\phi(T)}{\tilde{\epsilon}}}$ arise at the RHS when dividing by $\mathrm{e}^{\frac{\phi(T)}{\tilde{\epsilon}}}$. However, under resonant conditions $\psi'(T) = \phi'(T) = \lambda_k(T)$ so that the system to be solved at order $\tilde{\epsilon}$ is

$$\left[A(T) + \lambda_k(T) H(T) \right] \mathbf{f}_1(T) = -\frac{d\mathbf{f}_0}{dT} + \mathbf{y}_0(T), \quad (12)$$

which is linear, non homogeneous, but singular because the coefficient matrix $[A(T) + \lambda_k(T)H(T)]$ is the same as order $\tilde{\epsilon}^0$. For this reason the RHS must satisfy the compatibility condition, i.e. the dot product between the RHS and the left eigenvector $\tilde{\mathbf{v}}_k$, corresponding to the eigenvalue λ_k that renders the system singular, has to be zero:

$$\tilde{\mathbf{v}}_k(T) \cdot \left(-\frac{d\mathbf{f}_0}{dT} + \mathbf{y}_0(T) \right) = 0. \quad (13)$$

By expanding the compatibility condition (13) and recalling that $\mathbf{f}_0(T) = c_k(T)\tilde{\mathbf{u}}_k(T)$, the following first-order non-homogeneous ordinary differential equation for the unknown $c_k(T)$ is derived

$$\tilde{\mathbf{v}}_k(T) \cdot \tilde{\mathbf{u}}_k(T)\frac{dc_k}{dT} + \tilde{\mathbf{v}}_k(T) \cdot \frac{d\tilde{\mathbf{u}}_k(T)}{dT}c_k$$
$$= \tilde{\mathbf{v}}_k(T) \cdot \mathbf{y}_0(T). \quad (14)$$

After introducing

$$p(T) = \left[\tilde{\mathbf{v}}_k(T) \cdot \frac{d\tilde{\mathbf{u}}_k(T)}{dT} \right] \Big/ \left[\tilde{\mathbf{v}}_k(T) \cdot \tilde{\mathbf{u}}_k(T) \right]$$

and

$$q(T) = \frac{[\tilde{\mathbf{v}}_k(T) \cdot \mathbf{y}_0(T)]}{[\tilde{\mathbf{v}}_k(T) \cdot \tilde{\mathbf{u}}_k(T)]},$$

equation (14) reduces to

$$\frac{dc_k}{dT} + p(T)c_k = q(T),$$

whose closed-form solution is

$$c_k(T) = \mathrm{e}^{-\int_{T_0}^{T} p(T')\, dT'} \int_{T_0}^{T} q(T'') \, \mathrm{e}^{\int_{T_0}^{T''} p(T')\, dT'}\, dT''$$

$$= \int_{T_0}^{T} q(T'') \, \mathrm{e}^{\int_{T}^{T''} p(T')\, dT'}\, dT''.$$

Once $c_k(T)$ is known, vector $\mathbf{f}_0(T) = c_k(T)\tilde{\mathbf{u}}_k(T)$ is retrieved. It should be noticed that $\mathbf{f}_0(T)$ is independent of the normalization chosen for $\tilde{\mathbf{u}}_k(T)$. By truncating the solution at order $\tilde{\epsilon}^0$, the state vector $\mathbf{x}(T)$ is finally obtained as $\mathbf{x}(T) = c_k(T)\tilde{\mathbf{u}}_k(T)\exp(\phi(T)/\tilde{\epsilon}) + \mathcal{O}(\tilde{\epsilon})$ or, after substituting the closed-form expression for $c_k(T)$,

$$\mathbf{x}(T) = \tilde{\mathbf{u}}_k(T) \int_{T_0}^{T} \left[\mathbf{r}(T'') \cdot \mathbf{y}_0(T'') \right] dT'' + \mathcal{O}(\tilde{\epsilon}), \quad (15)$$

where

$$\mathbf{r}(T'') = \frac{\tilde{\mathbf{v}}_k(T'')\mathrm{e}^{\frac{\phi(T)}{\tilde{\epsilon}}}}{\tilde{\mathbf{v}}_k(T'') \cdot \tilde{\mathbf{u}}_k(T'')}$$
$$\times \exp\left(\int_{T}^{T''} \frac{\tilde{\mathbf{v}}_k(T') \cdot d\tilde{\mathbf{u}}_k(T')/dT}{\tilde{\mathbf{v}}_k(T') \cdot \tilde{\mathbf{u}}_k(T')}\, dT' \right).$$

Equation (15) compactly expresses the state vector $\mathbf{x}$ as a function of the right eigenvector $\tilde{\mathbf{u}}_k$ (computed at order $\tilde{\epsilon}^0$ and arbitrarily normalized) multiplied by the integral of the dot product between the resonant forcing source $\mathbf{y}_0$ and a weight $\mathbf{r}$. The latter function, $\mathbf{r}$, is otherwise known as "receptivity" because it describes the sensitivity of the solution to the forcing $\mathbf{y}_0$. $\mathbf{r}$ contains the left eigenvector $\tilde{\mathbf{v}}_k$ of the eigenvalue problem (11), and therefore can be interpreted also as the solution of the adjoint problem derived from (11).

5 Non-homogeneous multiple scales applied to the linearized Navier-Stokes equations

The necessity to solve the resonant problem governed by equation (7) and the slow dependence of the linear operator $L_{\epsilon\delta}$ on the streamwise coordinate suggest the use of the multiple scales.

A small parameter $\tilde{\epsilon}$, accounting for the scale separation between the streamwise variation of the base flow and the streamwise oscillation of the perturbation can be introduced in a number of ways. If the scale of the oscillation is assumed to be comparable to the boundary-layer thickness, it may seem natural to identify $\tilde{\epsilon}$ with $R^{-1/2}$. However, doing so leads to an inviscid leading-order problem, which turns out to be non-uniformly valid across the boundary layer. This

non-uniformity is accounted for in multiple-deck theory, which eventually shows that $\tilde{\epsilon}$ is *not* $\mathcal{O}(R^{-1/2})$.

In a different approach, which we adopt here, $\tilde{\epsilon}$ and R are treated as mutually independent parameters. This is actually the case if the base flow is embedded in a larger class of problems, possibly including volume forces. In such a larger class of problems the streamwise and normal scales of variation of the base flow are untied to the Reynolds number (for instance, in a truly parallel flow the streamwise scale is infinite despite both the normal scale and Reynolds number are finite), whereas the perturbation wavelength is a complicated function of the Reynolds number which is implicitly accounted for by keeping all the R-dependent terms in the equations, just as would happen in truly parallel flow. The expansion parameter $\tilde{\epsilon}$ is the ratio between this wavelength and the typical longitudinal scale of the base flow. Of course the accuracy of the solution cannot be harmed by keeping all the R-dependent terms in the equations while performing an expansion in $\tilde{\epsilon}$ only.

With a, b, c being the forcing terms as defined in (8), system (7) can be expanded similarly to (16).

$$(\hat{u}_{\epsilon\delta})_{\hat{x}} + (\hat{v}_{\epsilon\delta})_{\hat{y}} + (\hat{w}_{\epsilon\delta})_{\hat{z}} = 0$$

$$(\hat{u}_{\epsilon\delta})_{\hat{t}} + \hat{U}(\hat{u}_{\epsilon\delta})_{\hat{x}} + \hat{u}_{\epsilon\delta}\hat{U}_{\hat{x}} + \hat{V}(\hat{u}_{\epsilon\delta})_{\hat{y}} + \hat{v}_{\epsilon\delta}\hat{U}_{\hat{y}}$$
$$\quad + \hat{W}(\hat{u}_{\epsilon\delta})_{\hat{z}} + \hat{w}_{\epsilon\delta}\hat{U}_{\hat{z}}$$
$$= -(\hat{p}_{\epsilon\delta})_{\hat{x}} + R^{-1}\big[(\hat{u}_{\epsilon\delta})_{\hat{x}\hat{x}} + (\hat{u}_{\epsilon\delta})_{\hat{y}\hat{y}} + (\hat{u}_{\epsilon\delta})_{\hat{z}\hat{z}}\big]$$
$$\quad - \tilde{\epsilon}a$$

$$(\hat{v}_{\epsilon\delta})_{\hat{t}} + \hat{U}(\hat{v}_{\epsilon\delta})_{\hat{x}} + \hat{u}_{\epsilon\delta}\hat{V}_{\hat{x}} + \hat{V}(\hat{v}_{\epsilon\delta})_{\hat{y}} + \hat{v}_{\epsilon\delta}\hat{V}_{\hat{y}}$$
$$\quad + \hat{W}(\hat{v}_{\epsilon\delta})_{\hat{z}} + \hat{w}_{\epsilon\delta}\hat{V}_{\hat{z}} \qquad\qquad (16)$$
$$= -(\hat{p}_{\epsilon\delta})_{\hat{y}} + R^{-1}\big[(\hat{v}_{\epsilon\delta})_{\hat{x}\hat{x}} + (\hat{v}_{\epsilon\delta})_{\hat{y}\hat{y}} + (\hat{v}_{\epsilon\delta})_{\hat{z}\hat{z}}\big]$$
$$\quad - \tilde{\epsilon}b$$

$$(\hat{w}_{\epsilon\delta})_{\hat{t}} + \hat{U}(\hat{w}_{\epsilon\delta})_{\hat{x}} + \hat{u}_{\epsilon\delta}\hat{W}_{\hat{x}} + \hat{V}(\hat{w}_{\epsilon\delta})_{\hat{y}} + \hat{v}_{\epsilon\delta}\hat{W}_{\hat{y}}$$
$$\quad + \hat{W}(\hat{w}_{\epsilon\delta})_{\hat{z}} + \hat{w}_{\epsilon\delta}\hat{W}_{\hat{z}}$$
$$= -(\hat{p}_{\epsilon\delta})_{\hat{z}} + R^{-1}\big[(\hat{w}_{\epsilon\delta})_{\hat{x}\hat{x}} + (\hat{w}_{\epsilon\delta})_{\hat{y}\hat{y}} + (\hat{w}_{\epsilon\delta})_{\hat{z}\hat{z}}\big]$$
$$\quad - \tilde{\epsilon}c.$$

It should be noted that the forcing terms appear multiplied by $\tilde{\epsilon}$, as explained for the one-dimensional resonant example in Sect. 4. Boundary conditions for system (16), which are derived from (4), provide a contri-

bution of order $\tilde{\epsilon}$ and read

$$\hat{u}_{\epsilon\delta}(\hat{x}, 0, \hat{z}) = -\tilde{\epsilon}h(\hat{x})\frac{\partial \hat{u}_{\epsilon}}{\partial \hat{y}}|_{\hat{y}=0}$$

$$\hat{v}_{\epsilon\delta}(\hat{x}, 0, \hat{z}) = -\tilde{\epsilon}h(\hat{x})\frac{\partial \hat{v}_{\epsilon}}{\partial \hat{y}}|_{\hat{y}=0} \qquad\qquad (17)$$

$$\hat{w}_{\epsilon\delta}(\hat{x}, 0, \hat{z}) = -\tilde{\epsilon}h(\hat{x})\frac{\partial \hat{w}_{\epsilon}}{\partial \hat{y}}|_{\hat{y}=0}.$$

Following the same steps as in the one-dimensional example (see Sect. 4 or the Appendix B), new coordinates are introduced, $x = \tilde{\epsilon}\hat{x}, y = \hat{y}, z = \tilde{\epsilon}\hat{z}, t = \hat{t}$ and the base flow is expressed in the new reference frame as

$$U(x, y, z) = \hat{U}(\hat{x}, \hat{y}, \hat{z})$$
$$V(x, y, z) = \hat{V}(\hat{x}, \hat{y}, \hat{z})/\tilde{\epsilon}$$
$$W(x, y, z) = \hat{W}(\hat{x}, \hat{y}, \hat{z}).$$

The generic quantity $\hat{q}(\hat{x}, \hat{y}, \hat{z}, \hat{t})$ (which corresponds to $\hat{u}, \hat{v}, \hat{w}$ or $\hat{p}$ previously introduced) is expanded as

$$\hat{q}(\hat{x}, \hat{y}, \hat{z}, \hat{t}) = \big(q_0(x, y) + \tilde{\epsilon}q_1(x, y)$$
$$\quad + \cdots\big)e^{\frac{i\theta(x)}{\tilde{\epsilon}} + i\beta z - i\omega t}, \qquad (18)$$

where $\theta(x)$ is related to the streamwise wavenumber α by $\alpha = d\theta/dx$, β is the spanwise wavenumber and ω the frequency. After introducing expression (18) together with its first and second derivatives in (16) and boundary conditions (17), the original resonant problem (7) is recast as two linear problems at orders $\tilde{\epsilon}^0$ and $\tilde{\epsilon}^1$ (in the multiple-scale small parameter $\tilde{\epsilon}$),

order $\tilde{\epsilon}^0$:

$$\boldsymbol{A}(\alpha, \omega, R)\mathbf{f}_{0\epsilon\delta} = 0$$

order $\tilde{\epsilon}^1$: $\qquad\qquad\qquad\qquad\qquad\qquad (19)$

$$\boldsymbol{A}(\alpha, \omega, R)\mathbf{f}_{1\epsilon\delta} = -\boldsymbol{H}(\alpha, R)\frac{d\mathbf{f}_{0\epsilon\delta}}{dx}$$
$$\qquad\qquad + \boldsymbol{C}(\alpha, R)\mathbf{f}_{0\epsilon\delta} + \mathbf{y}_{\epsilon\delta},$$

where vectors

$$\mathbf{f}_{0\epsilon\delta} = \big[u_{0\epsilon\delta}(x, y), v_{0\epsilon\delta}(x, y), w_{0\epsilon\delta}(x, y), p_{0\epsilon\delta}(x, y)\big]$$

and

$$\mathbf{f}_{1\epsilon\delta} = \big[u_{1\epsilon\delta}(x, y), v_{1\epsilon\delta}(x, y), w_{1\epsilon\delta}(x, y), p_{1\epsilon\delta}(x, y)\big]$$

are the unknowns of the problem, and matrices A, H and C are defined in Appendix B (A is the well-known Orr–Sommerfeld operator). In what follows, vectors and matrices will be indicated as a function of x only, even though they do depend on y as well. Equations (19) are the generalization of (11) and (12) to a multi-dimensional problem.

The order-0 equation in system (19) is the classical Orr–Sommerfeld problem for the spatial-stability analysis. Given ω_{TS} and R, the wavenumber α_{TS} of the most unstable mode (TS wave) and its corresponding eigenvector $\mathbf{f}_{0\epsilon\delta}$ are obtained from the dispersion relation $D(\alpha, \omega, R) = 0$, which is equivalent to imposing $\det(A) = 0$. As noticed in Sect. 4, $\mathbf{f}_{0\epsilon\delta}$ is not unique and its normalization is arbitrary, i.e. $\mathbf{f}_{0\epsilon\delta} = c(x)\tilde{\mathbf{f}}_{0\epsilon\delta}$, where $c(x)$ is an unknown multiplicative function to be determined through the solvability condition at order $\tilde{\epsilon}^1$.

At order $\tilde{\epsilon}^1$, the forcing $\mathbf{y}_{\epsilon\delta}$ has, in general, a wide spectrum and therefore does not need to be represented by wave packets. However, since we are interested in the resonant problem for which the wavenumber and frequency of the forcing tend to the TS ones, we assume that the velocity disturbances at orders ϵ and δ are in the form

$$\epsilon\big[u_\epsilon(x, y), v_\epsilon(x, y), w_\epsilon(x, y)\big]$$
$$\times \exp\left(i \int \alpha_\epsilon dx' - i\omega_\epsilon t\right)$$

and

$$\delta\big[u_\delta(x, y), v_\delta(x, y), w_\delta(x, y)\big]$$
$$\times \exp\left(i \int \alpha_\delta dx' - i\omega_\delta t\right),$$

so that their coupling at order $\epsilon\delta$ provides the forcing

$$\mathbf{y}_{\epsilon\delta} = -\begin{pmatrix} 0 \\ i\alpha_\delta u_\epsilon u_\delta + i\alpha_\epsilon u_\delta u_\epsilon + v_\epsilon(u_\delta)_y + v_\delta(u_\epsilon)_y + i\beta w_\epsilon u_\delta + i\beta w_\delta u_\epsilon \\ i\alpha_\delta u_\epsilon v_\delta + i\alpha_\epsilon u_\delta v_\epsilon + v_\epsilon(v_\delta)_y + v_\delta(v_\epsilon)_y + i\beta w_\epsilon v_\delta + i\beta w_\delta v_\epsilon \\ i\alpha_\delta u_\epsilon w_\delta + i\alpha_\epsilon u_\delta w_\epsilon + v_\epsilon(w_\delta)_y + v_\delta(w_\epsilon)_y + i\beta w_\epsilon w_\delta + i\beta w_\delta w_\epsilon \end{pmatrix}. \quad (20)$$

The compatibility condition required to solve the singular system at order $\tilde{\epsilon}^1$ in (19) provides the equation for c

$$\frac{dc}{dx} + \frac{a_2}{a_1}c = \frac{\mathbf{f}^* \cdot \mathbf{y}_{\epsilon\delta}}{a_1},$$

similar to (14), where $a_1 = \mathbf{f}^* \cdot H\tilde{\mathbf{f}}_{0\epsilon\delta}$ and $a_2 = \mathbf{f}^* \cdot H d\tilde{\mathbf{f}}_{0\epsilon\delta}/dx + C\tilde{\mathbf{f}}_{0\epsilon\delta}$. The solution at a final streamwise location x_f is

$$c(x_f) = \int_{x_0}^{x_f}\left[\frac{\mathbf{f}^*(x) \cdot \mathbf{y}_{\epsilon\delta}(x)}{a_1(x)}\right.$$
$$\left. \times \exp\left(-\int_x^{x_f} \frac{a_2(x')}{a_1(x')} dx'\right)\right]dx,$$

where x_0 is a certain initial (upstream) station. Coefficient a_2 accounts for the non-parallel effects. In the case of parallel-flow assumptions ($U = U(y)$ and $V = W = 0$) a_2 is zero because $d\tilde{\mathbf{f}}_{0\epsilon\delta}/dx = 0$ (the vector $\tilde{\mathbf{f}}_{0\epsilon\delta}$ is constant), and matrix $C = 0$ (it con-

tains the derivatives of U with respect to x and the V-component of the base flow).

By considering only the $\mathcal{O}(\tilde{\epsilon}^0)$ contribution to the multiple-scale expansion, the solution at order $\epsilon\delta$ is $\mathbf{f}_{\epsilon\delta}(x_f) = c(x_f)\tilde{\mathbf{f}}_{0\epsilon\delta}(x_f) \exp(i\int_{x_0}^{x_f} \alpha\, dx') + \mathcal{O}(\tilde{\epsilon})$, or, after substituting $c(x_f)$,

$$\mathbf{f}_{\epsilon\delta}(x_f) = \tilde{\mathbf{f}}_{0\epsilon\delta}(x_f) \int_{x_0}^{x_f} \mathbf{r}(x) \cdot \mathbf{y}_{\epsilon\delta}(x)\, dx + \mathcal{O}(\tilde{\epsilon}), \quad (21)$$

with

$$\mathbf{r}(x) = \frac{\mathbf{f}^*(x)}{a_1(x)} \times e^{i \int_{x_0}^{x_f} \alpha\, dx' - \int_x^{x_f} \frac{a_2}{a_1} dx'}. \quad (22)$$

Vector $\mathbf{f}_{\epsilon\delta}$ in (21) includes the eigenvector $\tilde{\mathbf{f}}_{0\epsilon\delta}$ at order $\tilde{\epsilon}^0$ and the integral of the dot product between the resonant forcing $\mathbf{y}_{\epsilon\delta}(x)$ and the vector $\mathbf{r}(x)$, which is the receptivity (sensitivity) of the solution to the forcing. It should be kept in mind that the solution $\mathbf{f}_{\epsilon\delta}(x_f)$, in general, is expressed by a convolution and not by a simple integral. The simplification to an integral originates from the fact that we are focusing on a specific

mode selected by the TS problem. $\mathbf{r}(x)$ can also be seen as a Green function, which is actually different from zero only in a narrow band. The multiple-scale approximation, introduced for a slowly varying flow field as opposed to a uniform one, is contained in the function $\mathbf{r}(x)$. No further hypotheses are required for the source term $\mathbf{y}_{\epsilon\delta}(x)$.

6 Interacting disturbances

6.1 Acoustic wave

We assume that the free-stream acoustic wave is plane and characterized by a streamwise velocity amplitude ϵ and frequency ω_ϵ. This wave, interacting with the boundary layer on the flat plate, induces a perturbation that can be described by the Navier-Stokes equations linearized about the base flow. Such a perturbation is independent of the streamwise and spanwise coordinates x and z, so that the governing equations reduce to

$$
\begin{aligned}
(v_\epsilon)_y &= 0 \\
-i\omega_\epsilon u_\epsilon + (p_\epsilon)_x - (u_\epsilon)_{yy}/R &= 0 \\
(p_\epsilon)_y &= 0,
\end{aligned}
\tag{23}
$$

with boundary conditions $u_\epsilon = v_\epsilon = 0$ at $y = 0$ and $u_\epsilon \to 1$, $v_\epsilon \to 0$ for $y \to \infty$. Being $(p_\epsilon)_x = i\omega_\epsilon$, this is equivalent to the well-known Stokes's second problem (the flow near an oscillating flat plate), for which $v_\epsilon = 0$ and u_ϵ depends on y alone,

$$
\begin{aligned}
&\epsilon \mathbf{v}_\epsilon(x, y) \exp(-i\omega_\epsilon t) \\
&\quad = \epsilon\big(1 - \exp(-\sqrt{-i\omega_\epsilon R}\, y), 0\big) \exp(-i\omega_\epsilon t).
\end{aligned}
$$

The governing equations for the acoustic wave disturbance can also be obtained by straightforwardly removing the x- and z-dependence in the OS operator (i.e. $\alpha = 0$ and $\beta = 0$). Therefore, equations (23) are the leading-order equations of a multiple-scale expansion in which the small parameter $\tilde\epsilon$ is $U_\infty/(\omega_\epsilon L)$ (L being a typical length in the streamwise direction and U_∞ the outer velocity). Since U_∞/ω_ϵ is on the same order as the streamwise scale for the TS waves, $\alpha = 0$ reduces the OS operator at order $\tilde\epsilon^0$ to the acoustic wave equations. Therefore, the small parameter in the multiple-scale expansion applied to the acoustic wave and the small parameter in the multiple-scale for the OS equation are on the same order of magnitude. If

$L \gg U_\infty/\omega_\epsilon$, the variation of the acoustic disturbance in the streamwise direction induced by the boundary-layer growth is negligible, and the multiple-scale expansion stopped at the leading order $\tilde\epsilon^0$ provides a good approximation.

6.2 Vorticity wave

In general, both longitudinal and spanwise vorticity can play a role in the receptivity process; here we focus on the second case. A complete three-dimensional vorticity disturbance can be considered by extending the present approach without any particular difficulties.

Let ϵ be the amplitude of the streamwise velocity disturbance and ω_ϵ its characteristic frequency. The main difference with the acoustic wave is that the vorticity wave is characterized by a certain spatial wavelength α_ϵ different from zero. As it is well known, vorticity waves are described by the continuous spectrum of the OS equation. However, in order to assign a quantitative value to receptivity, it is necessary to define the amplitude of the perturbation through a coefficient characterizing its behavior in the outer (inviscid) region, as detailed below.

Among the components of the continuous spectrum of the OS equation, we need only consider those with $\alpha_\epsilon \ll 1/\delta^*$, because perturbations with wavelengths comparable to the boundary-layer thickness ($\alpha_\epsilon \approx 1/\delta^*$) decay over a longitudinal distance which is of the same order as the flat-plate length, i.e. long before reaching the leading edge. For this reason waves with $\alpha_\epsilon \geq 1/\delta^*$ will not be present in practical flight conditions.

The inviscid outer flow allows non-zero vorticity disturbances that behave as $e^{-i\omega_\epsilon t + i\alpha_\epsilon x}$, with $\alpha_\epsilon = \omega_\epsilon/U_\infty$. This free-stream traveling disturbance induces a perturbation in the boundary layer, where the viscous equations are valid. The boundary conditions for the boundary-layer disturbance are homogeneous at the wall, whereas for $y \to \infty$ the solution must match the asymptotic behavior of the outer flow. Matching must be provided between the viscous and inviscid regions.

In the inviscid (outer) region, a certain unsteady spanwise vorticity distribution $\zeta = \zeta(y, t)$ given at $x = 0$ evolves in time as $\zeta(y, t - x/U_e)$. By introducing the stream-function variable ψ_ϵ, so that $u_\epsilon = \partial\psi_\epsilon/\partial y$ and $v_\epsilon = -\partial\psi_\epsilon/\partial x$, the boundary condition at the wall becomes $\psi_\epsilon = 0$. In the proximity

of the wall, the solution behaves (in y) as $\psi_\epsilon(y) = Cy$ where $C = f(t - x/U_e)$ or, in Fourier components, $C = e^{i\omega_\epsilon(t - x/U_e)}$. If we limit our analysis to disturbances of wavelengths much larger than the boundary-layer thickness, then this is precisely the behavior that we expect at the matching with the outer solution, and allows us to assign a certain intensity to the perturbation as a function of the coefficient C, which is, indeed, the velocity of the outer (inviscid) flow evaluated at the wall. It should be noted that, in order to provide a quantitative value of receptivity (which must be independent of multiplicative constants), it is necessary to assign the intensity of the perturbation through a well-determined property of the outer solution.

As an alternative to the linearized boundary-layer equations, the matching with the viscous region can employ the Orr-Sommerfeld equation (more suitable for the present analysis). The solutions of the OS equation corresponding to the continuous spectrum, in the limit $y \to \infty$, are unique up to a multiplicative constant for every pair (ω, α). Such solutions contain the terms

$$e^{(-\alpha y)}, \qquad e^{\sqrt{\alpha^2 + iR(\alpha U_e - \omega)}\,y},$$
$$e^{-\sqrt{\alpha^2 + iR(\alpha U_e - \omega)}\,y}$$

in certain proportions and, therefore, can behave differently as $y \to \infty$. Also the solutions of the linearized boundary-layer equations are unique up to a multiplicative constant, contain the terms

$$1, \qquad e^{\sqrt{iR(\alpha U_e - \omega)}\,y}, \qquad e^{-\sqrt{iR(\alpha U_e - \omega)}\,y},$$

and, for the same reasons as for the OS solutions, can behave differently as $y \to \infty$.

The dispersion relation of the outer-region waves must now be considered. For the OS equation, the outer dispersion relation $\alpha^2 + iR(\alpha U_e - \omega) = 0$ ensures that the solution behaves (in y) as $C_1 + C_2 y + C_3 e^{-\alpha y}$, (whereas for the boundary-layer equations the condition $\alpha U_e - \omega = 0$ implied that the solution behaves as $C_1 + C_2 y + C_3 y^2$). In both cases it is possible to normalize the solution such that $C_2 = 1$. Indeed, this is always true for the boundary-layer case, whereas for the OS case, in general, a wave packet depending also on the spanwise wavenumber β should be considered. However, since a disturbance can reach the leading edge before decaying only if β is small, the present analysis ($\beta = 0$) is satisfactory.

We consider the OS approach and compute the wavenumber of the vorticity wave from the outer dispersion relation $\alpha^2 + iR(\alpha U_e - \omega) = 0$ as

$$\alpha_\epsilon = \frac{-iU_e + i\sqrt{U_e^2 - 4i\omega_\epsilon R^{-1}}}{2R^{-1}}. \tag{24}$$

Having set $C_2 = 1$, the asymptotic solution becomes

$$\psi_\epsilon = (C_1 + y + C_3 e^{-\alpha_\epsilon y})e^{i(\alpha_\epsilon x - \omega_\epsilon t)},$$

which implies:

$$u_\epsilon = \frac{\partial \psi_\epsilon}{\partial y} = (1 - \alpha_\epsilon C_3 e^{-\alpha_\epsilon y})e^{i(\alpha_\epsilon x - \omega_\epsilon t)}$$

$$v_\epsilon = -\frac{\partial \psi_\epsilon}{\partial x} = -i\alpha_\epsilon(C_1 + y + C_3 e^{-\alpha_\epsilon y})e^{i(\alpha_\epsilon x - \omega_\epsilon t)}.$$

The boundary conditions for $y \to \infty$, therefore, reduce to

$$u_\epsilon \to (1 - \alpha_\epsilon C_3 e^{-\alpha_\epsilon y})e^{i(\alpha_\epsilon x - \omega_\epsilon t)}$$
$$v_\epsilon \to -i\alpha_\epsilon(C_1 + y + C_3 e^{-\alpha_\epsilon y})e^{i(\alpha_\epsilon x - \omega_\epsilon t)}, \tag{25}$$

with C_1 and C_3 free constants. It should be noted that all of the above analysis serves only the purpose of assigning a precise value to the multiplicative constant, whereas the behavior for $y \to \infty$ is a priori determined by the OS solution corresponding to the continuous spectrum.

The governing equations for the vorticity wave are the same as for the OS problem, with conditions (25) replacing the classical homogeneous boundary conditions at infinity. This is equivalent to solving the leading-order equations of the multiple-scale expansion. The condition that guarantees a good approximation at the leading order $\tilde{\epsilon}^0$ is $L \gg U_\infty/\omega_\epsilon$, where L is the typical streamwise length on which the boundary layer evolves and $U_\infty/\omega_\epsilon = 1/\alpha_\epsilon$ is the typical length on which the vorticity perturbation evolves.

Contrary to the OS case, however, the problem is nonsingular because α_ϵ and ω_ϵ are not simultaneously α_{TS} and ω_{TS}. After discretization, the governing equations and boundary conditions can formally be written as $A(\alpha_\epsilon, \omega_\epsilon, R)\mathbf{f}_\epsilon(x) = \mathbf{y}_\epsilon(x)\exp(i\int\alpha_\epsilon\,dx')$, where A is the OS operator, $\mathbf{f}_\epsilon(x)$ is the solution as a function of x (the y-dependence has already been considered in the discretization), and $\mathbf{y}_\epsilon(x)$ accounts only for the non homogeneous boundary conditions at infinity (25). The vorticity-wave velocity disturbance is

ultimately expressed as

$$\epsilon \mathbf{v}_\epsilon(x, y) \exp(-i\omega_\epsilon t)$$

$$= \epsilon \big(u_\epsilon(y), v_\epsilon(y)\big) \exp\left(i \int \alpha_\epsilon \, dx' - i\omega_\epsilon t\right).$$

6.3 Wall roughness

The wall-roughness shape is described by a function $y = \delta h(x)$, where δ is the typical roughness scale and $h(x)$ is an order-one function. In principle, when decomposed in Fourier series, $h(x)$ has a wide wavenumber spectrum. However, resonance between the TS wave and the nonlinear mixing of disturbances occurs only for a specific value of the wall-roughness wavenumber. Therefore, we focus on a particular α_δ, keeping in mind that the analysis can be performed for different wavenumbers.

We express the steady perturbation induced in the boundary layer by the wall roughness as a wave in the form $(u(x, y), v(x, y), w(x, y))e^{i \int \alpha_\delta dx'}$, where α_δ is related to the inverse of the typical roughness wavelength. The governing equations can be obtained from the multiple-scale approximation limited to the leading order $\tilde{\epsilon}^0$. A good approximation is provided as long as $L \gg 1/\alpha_\delta$, where L is the scale of boundary-layer variation and $1/\alpha_\delta$ is the scale on which the wall-roughness induced perturbation varies. Formally, the OS operator is employed, but the problem is solved for $\omega_\delta = 0$ (the perturbation is steady) and with non-homogeneous boundary conditions originating from the linearization at the wall:

$$u_{0\delta}(x, 0) = -h(x)\frac{\partial U}{\partial y}\bigg|_{y=0} e^{-i \int \alpha_\delta dx'}$$

$$v_{0\delta}(x, 0) = -h(x)\frac{\partial V}{\partial y}\bigg|_{y=0} e^{-i \int \alpha_\delta dx'}$$

$$w_{0\delta}(x, 0) = -h(x)\frac{\partial W}{\partial y}\bigg|_{y=0} e^{-i \int \alpha_\delta dx'}.$$

After the discretization of the equations and boundary conditions, the problem at order δ reduces to the linear system $A(\alpha_\delta, 0, R)\mathbf{f}_\delta(x) = \mathbf{y}_\delta(x)h(x)\exp(-i \int \alpha_\delta dx')$, where A is the OS operator evaluated at $\alpha = \alpha_\delta$ and $\omega = 0$, $\mathbf{f}_\delta(x)$ is the solution as a function of x (the y-dependence has already been considered in the discretization), and $\mathbf{y}_\delta(x)$ is nonzero only because of the terms $-(\partial U/\partial y)|_{y=0}$, $-(\partial V/\partial y)|_{y=0}$ and $-(\partial W/\partial y)|_{y=0}$ stemming from the boundary conditions at the wall.

6.4 Possible disturbance interactions

The disturbances modeled in the previous sections cannot resonate singularly with TS waves. For example, the wavenumber of an acoustic wave, in the incompressible case, is zero and thus it can never be close to α_{TS} (the frequency, however, could be in the range of ω_{TS}). The same happens for the wall vibration disturbance, for which $\alpha = 0$. Vorticity waves, on the other hand, are perturbations characterized by both wavenumber and frequency different from zero; however $\alpha = \omega/U_\infty$ is far from α_{TS}. Wall roughness, being stationary, cannot excite TS waves, at least as long as swept wings are not considered.

On the other hand, a resonant wave with wavenumber and frequency in the TS range can originate at order $\epsilon\delta$, via nonlinear interaction between the disturbances at orders ϵ and δ. Resonance conditions require $\alpha_\delta + \alpha_\epsilon \approx \alpha_{TS}$ and $\omega_\delta + \omega_\epsilon \approx \omega_{TS}$, so that only specific coupling between perturbations can effectively satisfy them. Possible interesting interactions are the following.

- Acoustic wave and wall roughness. The acoustic wave is solved at order ϵ and the wall roughness at order δ. $\alpha_\epsilon = 0$ and $\omega_\delta = 0$, so that resonance is guaranteed by $\alpha_\delta \approx \alpha_{TS}$ and $\omega_\epsilon \approx \omega_{TS}$. The boundary conditions to be used at the wall, after the linearization, are (4), which at order $\epsilon\delta$ include the first derivative of the Stokes's solution at the wall.
- Vorticity wave and wall roughness. The vorticity wave perturbation is computed at order ϵ and the wall roughness at order δ. Since the vorticity-wave dispersion relation allows $\alpha_\epsilon \neq 0$ and $\omega_\epsilon \neq 0$, resonance conditions are $\alpha_\delta + \alpha_\epsilon \approx \alpha_{TS}$ and $\omega_\epsilon \approx \omega_{TS}$. The correct boundary conditions at the wall are still described by the fourth equation in (4), so that the first derivative of the vorticity wave is employed at the wall.
- Acoustic wave and vorticity wave. The acoustic wave, solved at order δ, is characterized by $\alpha_\delta = 0$ and $\omega_\delta \neq 0$. The vorticity wave, on the contrary, allows both $\alpha_\epsilon \neq 0$ and $\omega_\epsilon \neq 0$, so that resonance can occur if $\alpha_\epsilon \approx \alpha_{TS}$ and $\omega_\delta + \omega_\epsilon \approx \omega_{TS}$. The combination between acoustic and vorticity waves provides homogeneous boundary conditions at the wall.

A subsection of Appendix C is devoted to the interaction between wall roughness and wall vibration.

For this case, we prove that the velocity disturbance at order $\epsilon\delta$ is the exact solution of the velocity perturbation induced by wall roughness on a wall vibrating in the normal direction, after introducing a new reference frame.

6.5 Wall receptivity coefficient

When the "tuning mechanism" that allows resonance with TS waves is due to wall roughness, the amplitude of the unstable perturbation can be related directly to the wall shape $h(x)$. Since the solution at order δ is a linear function of $h(x)$ (through the boundary conditions), so is the solution at order $\epsilon\delta$. This allows us to rewrite the forcing vector $\mathbf{y}_{\epsilon\delta}$ appearing in (19) at order $\tilde{\epsilon}$ as $\mathbf{y}_{\epsilon\delta}(x) = \tilde{\mathbf{y}}_{\epsilon\delta}(x)h(x)$, where $\tilde{\mathbf{y}}_{\epsilon\delta}(x) = \mathbf{y}_{\epsilon\delta}(x)/h(x)$. The integral in (21) becomes $\int_{x_0}^{x_f} \mathbf{r}(x) \cdot \mathbf{y}_{\epsilon\delta}(x)\,dx = \int_{x_0}^{x_f} \mathbf{r}(x) \cdot \tilde{\mathbf{y}}_{\epsilon\delta}(x)h(x)\,dx = \int_{x_0}^{x_f} r_h(x)h(x)\,dx$, where $r_h(x)$ is a scalar function denoting the dot product $\mathbf{r}(x) \cdot \tilde{\mathbf{y}}_{\epsilon\delta}(x)$ (it should be kept in mind that vectors depend also on y, here omitted in order to keep the notation lighter). Equation (21) can now be recast in the following form, where the linear dependence on the wall shape $h(x)$ is emphasized,

$$\mathbf{f}_{\epsilon\delta}(x_f) = \tilde{\mathbf{f}}_{0\epsilon\delta}(x_f) \int_{x_0}^{x_f} r_h(x)h(x)\,dx + \mathcal{O}(\tilde{\epsilon}). \qquad (26)$$

The reduction to a simple integral occurs because we are focusing on a single mode selected by the TS wave. More generally, the exciting source $\mathbf{y}_{\epsilon\delta}(x)$, due to the nonlinear interaction between wall roughness and other disturbances, can be written, using the Green function $\mathbf{g}$, as $\mathbf{y}_{\epsilon\delta}(x) = \int_{x_0}^{x_f} \mathbf{g}(x, x')h(x')\,dx'$. The solution $\mathbf{f}_{\epsilon\delta}$, when employing $\mathbf{g}$, is

$$\mathbf{f}_{\epsilon\delta}(x_f) = \tilde{\mathbf{f}}_{0\epsilon\delta}(x_f)\left[\int_{x_0}^{x_f} \int_{x_0}^{x_f} \mathbf{r}(x)\mathbf{g}(x, x')h(x')\,dx'\,dx \right]$$
$$\times \exp(-i\omega_\epsilon t) + \mathcal{O}(\tilde{\epsilon}),$$

and therefore more complicated than the simple integral (26).

By introducing the x-dependent coefficient

$$\hat{r}_h = \frac{\mathbf{f}^* \cdot \tilde{\mathbf{y}}_{\epsilon\delta}}{a_1} = \frac{\mathbf{f}^* \cdot \tilde{\mathbf{y}}_{\epsilon\delta}}{\mathbf{f}^* \cdot [\mathbf{H}\tilde{\mathbf{f}}_{0\epsilon\delta}]}, \qquad (27)$$

and by recalling the definition of $\mathbf{r}(x)$ as in (22), $a_1 = \mathbf{f}^* \cdot \mathbf{H}\tilde{\mathbf{f}}_{0\epsilon\delta}$ and $a_2 = \mathbf{f}^* \cdot \mathbf{H}d\tilde{\mathbf{f}}_{0\epsilon\delta}/dx + \mathbf{C}\tilde{\mathbf{f}}_{0\epsilon\delta}$ (see Sect. 5), the solution $\mathbf{f}_{\epsilon\delta}(x_f)$ in (26) becomes

$$\mathbf{f}_{\epsilon\delta}(x_f) = \tilde{\mathbf{f}}_{0\epsilon\delta}(x_f)$$
$$\times \int_{x_0}^{x_f} \hat{r}_h(x)\, \mathrm{e}^{i \int_{x_0}^{x_f} \alpha\,dx' - \int_x^{x_f} \frac{a_2}{a_1}\,dx'} h(x)\,dx. \qquad (28)$$

If the eigensolution $\tilde{\mathbf{f}}_{0\epsilon\delta}(x_f)$ in (28) has been normalized in such a way that $\max|\tilde{u}_{0\epsilon\delta}(x_f)| = 1$ ($\tilde{\mathbf{f}}_{0\epsilon\delta} = [\tilde{u}_{0\epsilon\delta}, \tilde{v}_{0\epsilon\delta}, \tilde{w}_{0\epsilon\delta}, \tilde{p}_{0\epsilon\delta}]^{\mathrm{T}}$), then the amplitude of $\mathbf{f}_{\epsilon\delta}(x_f)$ (defined as the maximum absolute value of the streamwise velocity component $\epsilon\delta u_{\epsilon\delta}(x_f, y)$ for $y \in [0; +\infty[$) is

$$A(x_f) = \left| \epsilon\delta\, \mathrm{e}^{i \int_{x_0}^{x_f} \alpha\,dx'} \int_{x_0}^{x_f} h(x)\hat{r}_h(x)\mathrm{e}^{-\int_x^{x_f} \frac{a_2}{a_1}\,dx'}\,dx \right|.$$

By introducing the *receptivity coefficient*

$$\bar{r}_h(x) = \hat{r}_h(x)\, \mathrm{e}^{-\int_x^{x_I} \frac{a_2}{a_1}\,dx'}, \qquad (29)$$

the final amplitude $A(x_f)$ can be further rearranged to emphasize its dependence on the integral between the wall shape $h(x)$ and the receptivity coefficient

$$A(x_f) = \left| \epsilon\delta \mathrm{e}^{i \int_{x_0}^{x_f} \alpha\,dx'} \mathrm{e}^{-\int_{x_I}^{x_f} \frac{a_2}{a_1}\,dx'} \int_{x_0}^{x_f} h(x)\bar{r}_h(x)\,dx \right|. \qquad (30)$$

Expression (30) is what we defined as the goal of a receptivity study because the final amplitude of the resonant wave $A(x_f)$ is formulated as a function of ϵ (the amplitude of the acoustic wave, vorticity wave or wall displacement due to the wall vibration), δ (the amplitude of the wall roughness), and $h(x)$ (the shape of the wall). An essential role is played by $\bar{r}_h(x)$, which is the receptivity to wall roughness or, in other words, the sensitivity of the final amplitude to the wall shape $h(x)$. Non-parallel flow effects in (30) are accounted for by the integral of a_2/a_1 in the exponential factors, whereas for parallel flows ($a_2 \equiv 0$) the amplitude (30) reduces to

$$A_{\mathrm{parallel}}(x_f) = \left| \epsilon\delta\, \mathrm{e}^{i \int_{x_0}^{x_f} \alpha\,dx'} \int_{x_0}^{x_f} h(x)\hat{r}_h(x)\,dx \right|.$$

It should be noticed that $\hat{r}_h(x)$ (see (27) for its definition) is the same receptivity coefficient computed for *parallel flows* by Crouch [19], Choudhari and Streett [17] and Hill [36] (these comparisons were carried out during the code verification).

For the interaction between the acoustic and vorticity waves $h(x) \equiv 0$ and the wall boundary conditions are homogeneous at all orders (ϵ—vorticity wave perturbation, δ—acoustic wave perturbation, and $\epsilon\delta$—resonant wave). The amplitude at the final station for this interaction is

$$A(x_\mathrm{f}) = \left| \epsilon\delta \mathrm{e}^{i \int_{x_0}^{x_\mathrm{f}} \alpha \, dx'} \mathrm{e}^{-\int_{x_\mathrm{I}}^{x_\mathrm{f}} \frac{a_2}{a_1} \, dx'} A_\mathrm{I} \right|,$$

where

$$A_\mathrm{I} = \int_{x_0}^{x_\mathrm{f}} \frac{\mathbf{f}^* \cdot \mathbf{y}_{\epsilon\delta}}{a_1} \mathrm{e}^{-\int_x^{x_\mathrm{f}} \frac{a_2}{a_1} \, dx'} \, dx.$$

7 Results

In this section we present the results for Blasius' boundary layer and consider each interaction described in Sect. 6. We systematically provide perturbations at order ϵ and δ, followed by the forcing terms originating from their interactions at order $\epsilon\delta$. Only the x- and y-momentum contributions to the left eigensolution $\mathbf{f}^*$ and to the forcing $\tilde{\mathbf{y}}_{\epsilon\delta}$ are shown, because they are the only effective (nonzero) terms in $\tilde{\mathbf{y}}_{\epsilon\delta}$. The receptivity coefficient is eventually plotted versus Reynolds number R for both parallel and nonparallel flows.

The wall-normal coordinate is normalized with the boundary-layer reference length $\delta_0 = \sqrt{\nu x_\mathrm{I}/U_\infty}$. The reference Reynolds number is $R_\mathrm{I} = U_\infty \delta_0/\nu = 557$, where $R = \sqrt{Re_x} = \sqrt{U_\infty x/\nu}$. The dimensionless frequency $F = \omega\nu/U_\infty^2$ has been chosen as $F = 5.9 \times 10^{-5}$, because for this value the amplification reaches a maximum with respect to F.
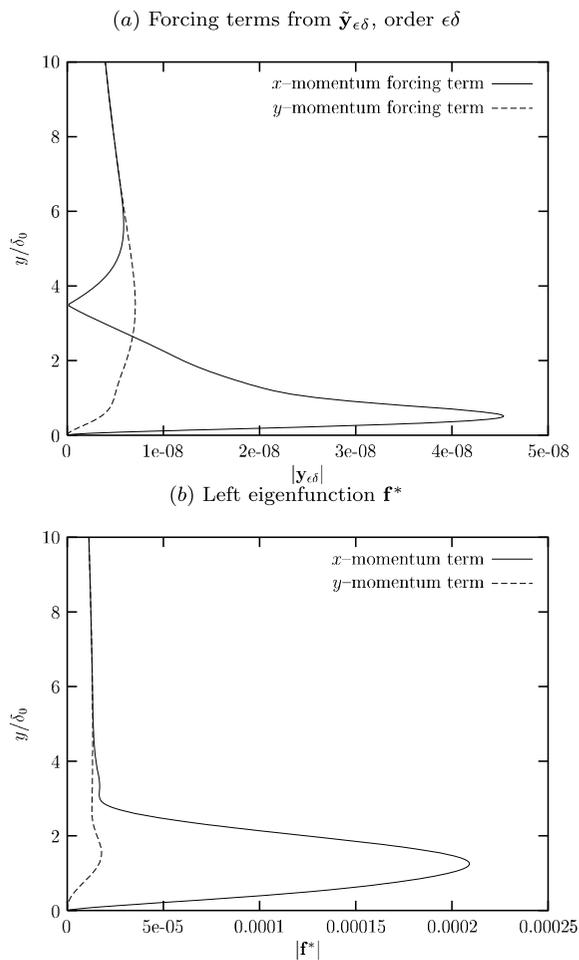
7.1 Acoustic wave–wall roughness interaction

Figure 2a shows the perturbation induced by the acoustic wave that travels in the free stream. The v-component is identically zero, whereas the u-component, independent of x, is Stokes's solution and becomes constant for $y/\delta_0 > 3$. Therefore, the main contribution of the acoustic perturbation to the forcing is confined within the boundary layer. Figure 2b reports the absolute value of the perturbation induced by the wall roughness and computed at $\alpha_\delta = \alpha_\mathrm{TS}$. Its main contribution is clearly localized inside the boundary layer too, with the solution going asymptotically to zero as $y/\delta_0 \to \infty$. The y-scale of the plot is limited to 10
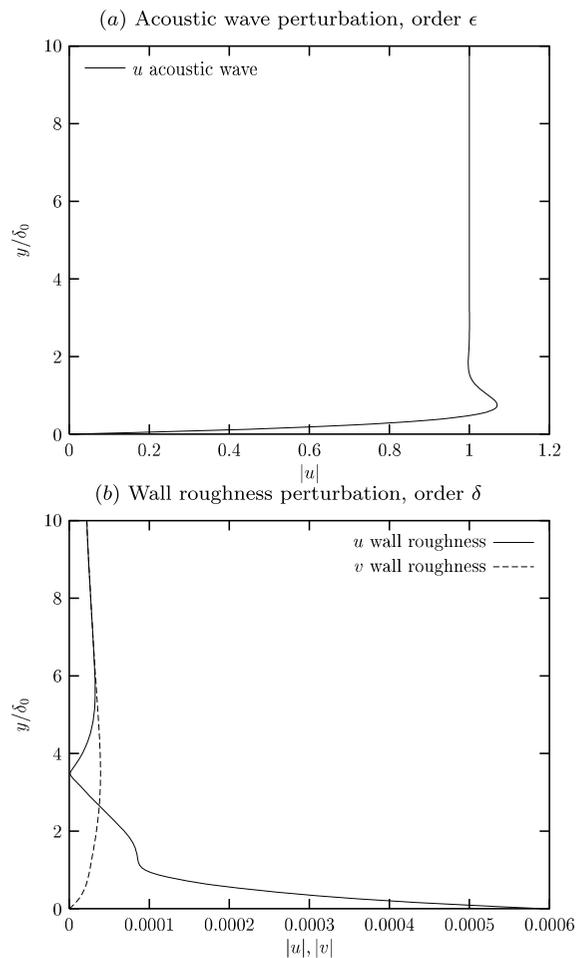
Fig. 2 Interacting perturbations at order ϵ and δ. $F = \omega\nu/U_\infty^2 = 5.9 \times 10^{-5}$, $R_\mathrm{I} = 557$

in order to disclose the most relevant features, which are significant only in the wall region, but the computations are performed for $y_\mathrm{max}/\delta_0 = 180$ (an outer zoom is proposed in Sect. 7.2 for the coupling between vorticity wave and wall roughness).

The interaction at order $\epsilon\delta$ between the previous perturbations produces the x- and y-momentum forcing terms reported in Fig. 3a (in absolute value). The strongest effect is provided by the x-momentum component, which is mainly localized inside the boundary layer, as a direct consequence of the perturbations shown in Fig. 2. It should be kept in mind that, at order $\epsilon\delta$, a contribution to the forcing comes also from the non homogeneous boundary condition at the wall. This contribution is not shown in Fig. 3a because the whole plot would not be visible due to the different orders of magnitude.

(a) Forcing terms from $\tilde{\mathbf{y}}_{\epsilon\delta}$, order $\epsilon\delta$

(a) Receptivity coefficient

(b) Left eigenfunction $\mathbf{f}^*$

(b) Ratio between receptivity coefficients

Fig. 3 Interaction between acoustic wave and wall roughness at order $\epsilon\delta$. $F = \omega/(\nu U_\infty^2) = 5.9 \times 10^{-5}$, $R_I = 557$

Fig. 4 Receptivity characteristics for the interaction between acoustic wave and wall roughness. $F = \omega\nu/U_\infty^2 = 5.9 \times 10^{-5}$, $R_I = 557$

The absolute value of the left eigenfunction $\mathbf{f}^*$ is reported in Fig. 3b. The x- and y-momentum contributions, which weight respectively the x- and y-momentum forcing, reach their maxima for $y/\delta_0 < 5$ suggesting that the receptivity coefficient originating from $\mathbf{f}^* \cdot \tilde{\mathbf{y}}_{\epsilon\delta}$ might be quite large.
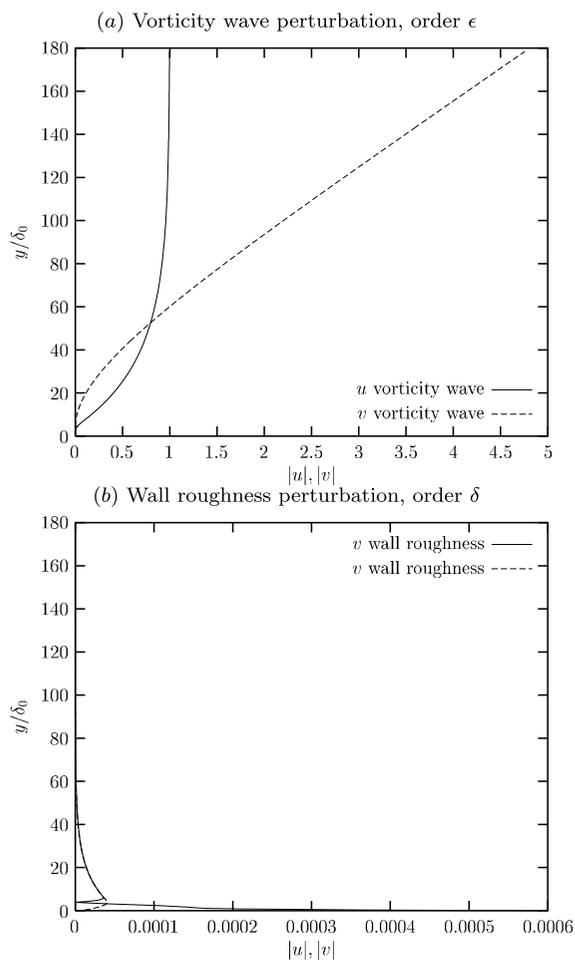
This conjecture is confirmed by Fig. 4a, where the absolute value of the receptivity coefficient is plotted under the assumptions of parallel and non parallel flows. In both cases it monotonically decreases with R. For parallel flows the coefficient reduces to $\hat{r}_h = \mathbf{f}^* \cdot \tilde{\mathbf{y}}_{\epsilon\delta}/a_1$, which can be directly compared with the results carried out by Crouch [19], Choudhari and Streett [17] and Hill [36]. For non parallel flows the receptivity coefficient is $\bar{r}_h = \hat{r}_h \exp(-\int_x^{x_I} \frac{a_2}{a_1} dx')$, where $a_2 \neq 0$ accounts for non-parallel effects. Since
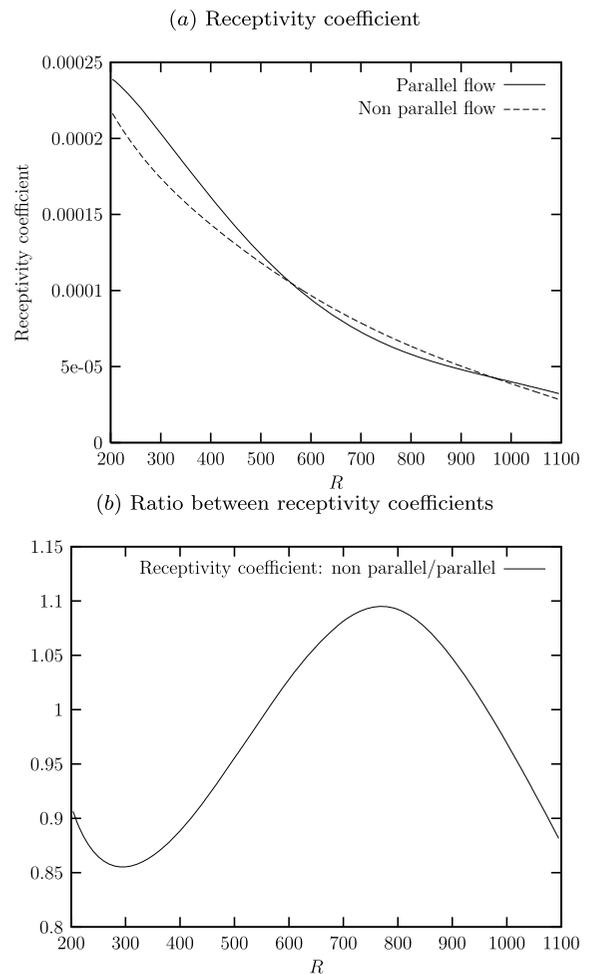
the integral in $\bar{r}_h$ is referred to the first neutral point, the values of the receptivity coefficients coincide at $R_I = 557$.

In order to better appreciate the contribution of the multiple scales in accounting for the boundary-layer growth, Fig. 4b shows the ratio $\bar{r}_h/\hat{r}_h = \exp(-\int_x^{x_I} \frac{a_2}{a_1} dx')$ between the non-parallel and parallel cases. Differences are on the order of 10 %, with peaks of 15 %, meaning that non-parallel flow effects introduced by this formulation play a non-negligible role even in Blasius' boundary layer. It should be noticed that for $F = \omega\nu/U_\infty^2 = 5.9 \times 10^{-5}$ non-parallel effects are not as strong as at higher frequencies (e.g. $F = 22 \times 10^{-5}$). For a more detailed discussion on non-parallel effects see Sect. 8.
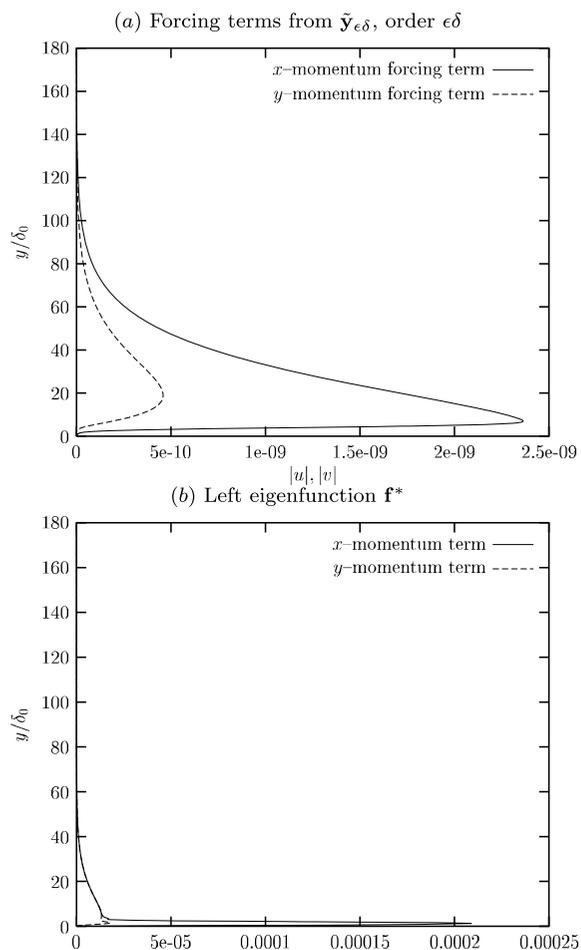
(a) Vorticity wave perturbation, order ϵ

(a) Forcing terms from $\tilde{\mathbf{y}}_{\epsilon\delta}$, order $\epsilon\delta$

(b) Wall roughness perturbation, order δ

(b) Left eigenfunction $\mathbf{f}^*$

Fig. 5 Interacting perturbations. $F = \omega\nu/U_\infty^2 = 5.9 \times 10^{-5}$, $R_I = 557$

Fig. 6 Interaction between vorticity wave and wall roughness at order $\epsilon\delta$. $F = \omega/(\nu U_\infty^2) = 5.9 \times 10^{-5}$, $R_I = 557$

7.2 Vorticity wave–wall roughness interaction

The perturbation induced by a vorticity wave, at the first neutral point, is plotted in Fig. 5a. For the conditions considered ($F = 5.9 \times 10^{-5}$ and $R_I = 557$), the wavenumber of TS waves (normalized with δ_0) is $\alpha_{TS}\delta_0 = 0.1$. The value of the spatial wavenumber, $\alpha_\epsilon\delta_0 = 0.0329$, to be used for the computation of the vorticity wave perturbation, is provided by (24). The wavenumber of the wall roughness perturbation is thus $\alpha_\delta\delta_0 = \alpha_{TS}\delta_0 - \alpha_\epsilon\delta_0 = 0.067$.

Figure 5a reveals that a very large value of y/δ_0 is required to achieve the asymptotic values of u and v. As $y/\delta_0 \to \infty$, the u-component reaches a constant value equal to 1 and the v-component behaves as a linear function of y/δ, as imposed by the boundary conditions (25). The main contribution of the vortic-

ity wave perturbation is outside the boundary layer, as it was observed by Wu [65], confirming the "shear sheltering" mechanism described by Hunt [37]. On the contrary, the perturbation due to wall roughness, which is reported in Fig. 5b, is mainly localized inside the boundary layer (this figure differs from Fig. 2b for the choice of the wavenumber α_δ).

The forcing terms caused by the interaction between vorticity wave and wall roughness are shown in Fig. 6a. In contrast with the interaction between acoustic wave and wall roughness, here the forcing is mainly localized outside the boundary layer. The x-momentum excitation peaks at about $y/\delta_0 = 8$, whereas the y-momentum reaches its maximum at about $y/\delta_0 = 20$. This is clearly due to the behavior of the velocity profiles induced by the vorticity wave, which do not go to zero as $y/\delta_0 \to \infty$. The pertur-
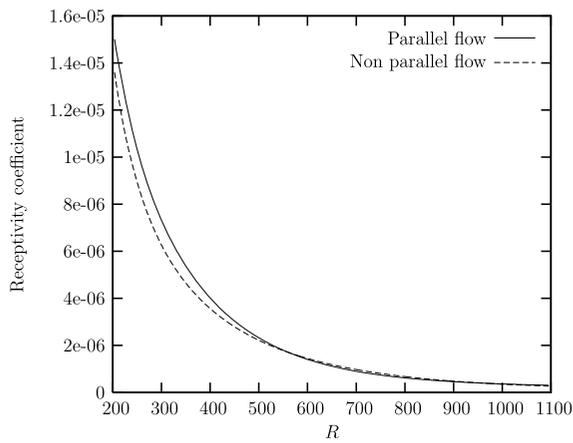
Fig. 7 Receptivity characteristics for the interaction between vorticity wave and wall roughness. $F = \omega \nu / U_\infty^2 = 5.9 \times 10^{-5}$, $R_I = 557$

Fig. 8 Interacting perturbations. $F = \omega \nu / U_\infty^2 = 5.9 \times 10^{-5}$, $R_I = 557$

bation due to the wall roughness, on the contrary, exponentially decays with the distance from the wall, driving the forcing term to zero as $y/\delta_0 \to \infty$. This exponential decay of $\tilde{\mathbf{y}}_{\epsilon\delta}$, however, is much slower than the decay observed for the interaction between an acoustic wave and wall roughness, so that a much larger distance from the wall is needed in order for it to vanish. The left eigenfunction $\mathbf{f}^*$ in Fig. 6b has the same characteristics as that in Fig. 3b, except to the y scale.

Parallel and non parallel receptivity coefficients are reported in Fig. 7. They monotonically decreases with R, just as in the acoustic wave–wall roughness interaction, and their ratio is the same as in Fig. 4b. Here, however, the slope of the curves is larger than in the previous case and the absolute values of the coefficients are about one order of magnitude smaller. Clearly, this is due to the fact that now the absolute value of the exciting terms in $\tilde{\mathbf{y}}_{\epsilon\delta}$ is one order of magnitude smaller than before, and to the fact that the forcing and the left eigenfunction peak at completely different distances from the wall (compare Figs. 6a and 6b). This feature could lead us to think that the interaction between vorticity wave and wall roughness is a negligible phenomenon (shear sheltering [37]). It can be true, but the final amplitude has to be yet multiplied by ϵ, the amplitude of the vorticity wave in the free-stream, and δ, the amplitude of the wall roughness. Therefore, the relative importance of one phenomenon with respect to the other depends on the actual level of the environmental disturbances involved.
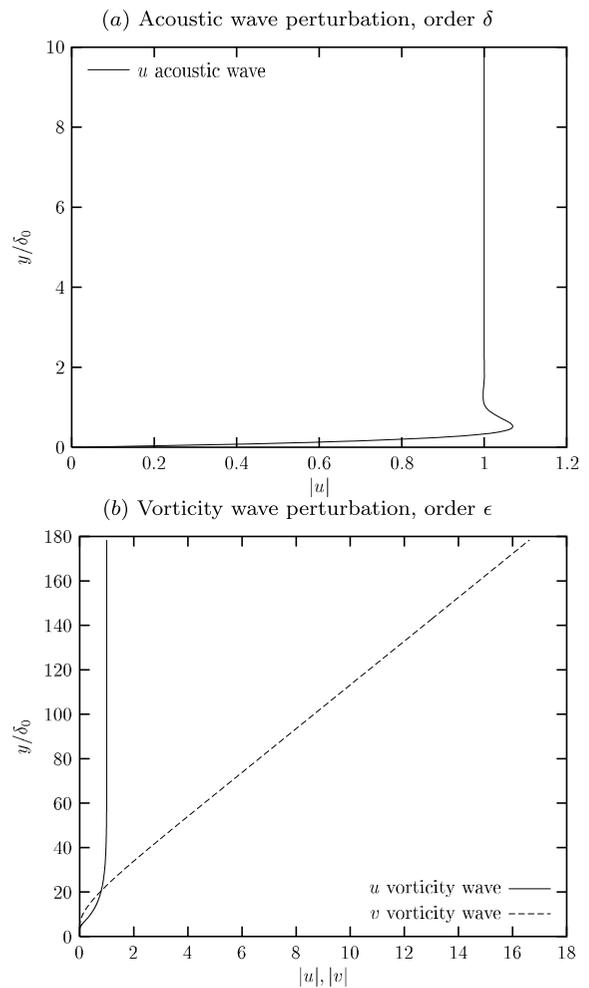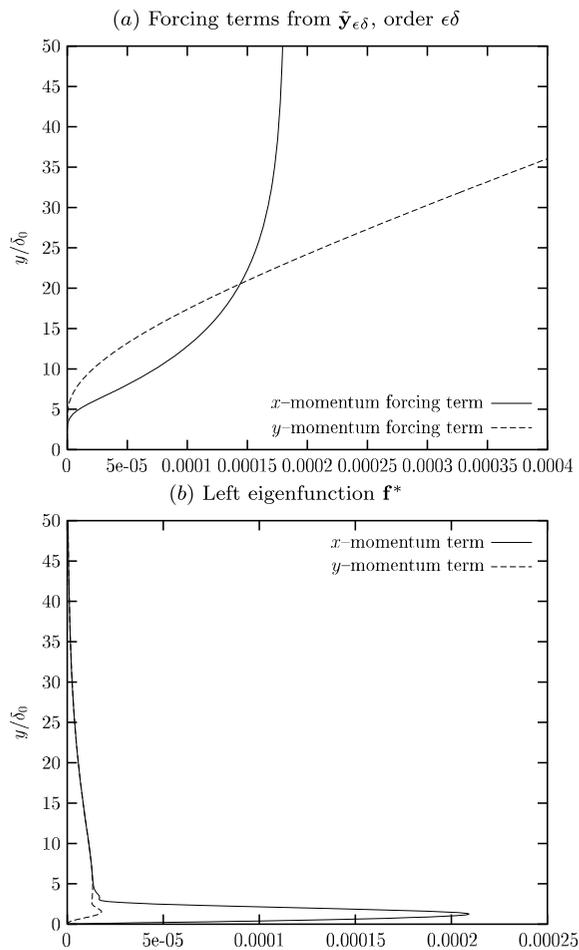
7.3 Acoustic wave–vorticity wave interaction

As for the previous interactions, we consider $F = 5.9 \times 10^{-5}$ and $R_I = 557$ obtaining $\alpha_{TS}\delta_0 = 0.1$. Since resonance occurs at $\alpha_\epsilon = \alpha_{TS}$, the wavenumber for the vorticity wave is $\alpha_\epsilon = 0.1$ whereas its frequency ω_ϵ is computed from equation (24), $\omega_\epsilon = (\alpha_\epsilon^2 + i\alpha_\epsilon U_e R)/(iR)$. Resonance imposes also $\omega_\epsilon + \omega_\delta = \omega_{TS}$, that gives the frequency of the acoustic wave $\omega_\delta = \omega_{TS} - \omega_\epsilon$.

The velocity perturbation due to the acoustic wave is shown in Fig. 8a. It should be noticed that this is not the same as in Fig. 2a because the frequency of the acoustic wave is different in the two cases. The general shape of the profile remains, however, unchanged. The vorticity wave perturbation in Fig. 8b shows a

Fig. 9 Interaction between acoustic wave and vorticity wave at order $\epsilon\delta$. $F = \omega/(\nu U_\infty^2) = 5.9 \times 10^{-5}$, $R_\mathrm{I} = 557$

quite remarkable difference compared with Fig. 5a. In the present case, the u-velocity component reaches the asymptotic value at $y/\delta_0 \approx 60$, while $u = 1$ was previously reached at $y/\delta_0 \approx 140$ (Fig. 5a).

The nonlinear interaction between the two disturbances of Fig. 8 is shown in Fig. 9a. The main difference with the previous cases is that the forcing does not vanish for $y/\delta_0 \to \infty$, as a consequence of the interacting-disturbances profiles, but behaves almost as the vorticity wave perturbation (a part from the scale).

On the contrary, the left eigenfunction $\mathbf{f}^*$ (Fig. 9b) reaches its maximum where the forcing term is very small and goes exponentially to zero where the forcing behaves as a constant (x-momentum) or linearly (y-momentum). For this reason the effects of the forcing are very limited.

8 A brief discussion on non-parallel effects

As mentioned in the introduction (see Sect. 2), during the historical development of receptivity theory, approaches different from multiple scales have been proposed in order to account for non-parallel effects. Among those, PSE has been successfully employed [1, 6, 35, 51] because this nonlinear partial differential equation incorporates the effects of streamwise divergence associated with boundary-layer non-parallelism. The aim of this brief discussion is to prove that results here obtained with multiple scales (MS) including non-parallel effects agree with PSE (when PSE converges) and other OS approaches.

Figure 10a reproduces Fig. 7 of Ref. [20], in which the OS formulation was employed and the hypothesis of parallel flow was relaxed by introducing the derivative of the disturbance amplitude with respect to the streamwise direction. The effective branch I amplitude A_I is reported as a function of the wall-roughness wavenumber α_w for $F = \omega\nu/U_\infty^2 = 5.6 \times 10^{-5}$, and $R = 550$ (these conditions are slightly different from those in Sect. 7). Full symbols refer to present calculations (MS), while empty symbols are data gathered from Ref. [20]. Only one point is, however, available for the PSE, $A_I = 51.7$ at $\alpha_\mathrm{w} = 0.174236$. From Fig. 10a it is clear that the quasi-parallel-flow approach introduced by Crouch [20] (empty squares) provides results that are much closer to the parallel, rather than non-parallel, computations carried out with the present multiple-scale approach. More specifically, without non parallel corrections to the amplitude (parallel-flow case, full squares), the maximum error is within 2.6 % and the optimal wavenumber α_w (for which the maximum of A_I is achieved) is about $\alpha_\mathrm{w} = 0.1714$, the same obtained by Crouch.

When non-parallel effects are accounted for (full circles in Fig. 10a), on the other hand, results differ from the quasi-parallel-flow approach, but agree very well with the values reported by Crouch [20] regarding the PSE, i.e. $A_I = 51.7$ at $\alpha_\mathrm{w} = 0.174236$. Unfortunately, from the data available in literature it is almost impossible to gather enough information for reconstructing a curve to plot in Fig. 10a for the PSE. However, it can be concluded that non-parallel effects influence the optimal α_w but not the value of the maximum A_I, which is quite insensitive.

In Fig. 10b we compare MS and PSE by plotting the N-factor (with non-parallel effects) as a function
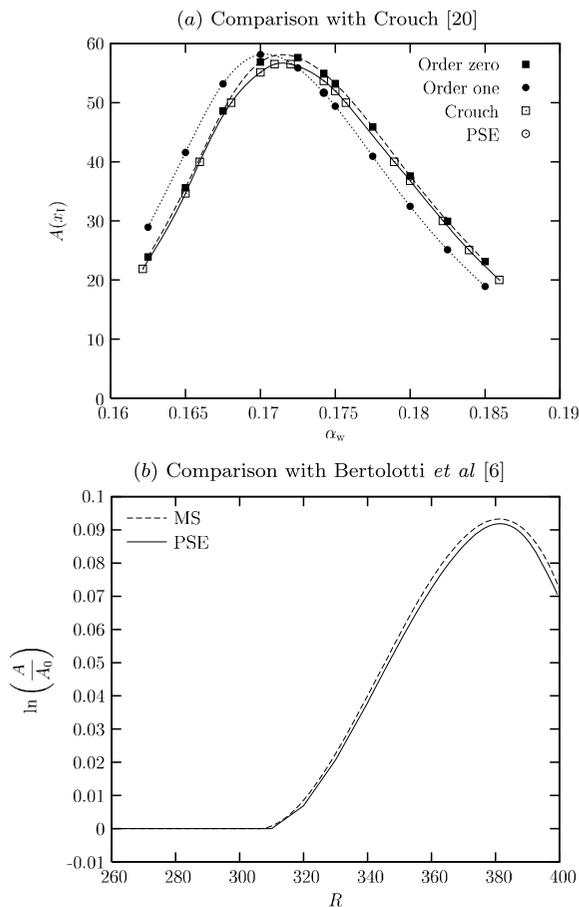
Fig. 10 Comparison with previously published results accounting for non-parallel effects. (**a**) Comparison with Crouch [20]: variation of the effective branch I amplitude A_I with α_w for $F = \omega\nu/U_\infty^2 = 5.6 \times 10^{-5}$, $R = 550$. (**b**) Comparison with Bertolotti et al. [6]: amplification curves as a function of R for $F = \omega\nu/U_\infty^2 = 22 \times 10^{-5}$, where non-parallel effects are very strong

of R for $F = \omega\nu/U_\infty^2 = 22 \times 10^{-5}$, which represents the worst-case scenario. In fact, Bertolotti et al. [6] showed that at high frequency non-parallel-flow effects play a non-negligible role in the Blasius' boundary layer (see Fig. 3a, p. 416, in Ref. [6]), whereas in the usual range of frequencies (i.e. for $F = 5 \times 10^{-5}$), linear stability theory, PSE and DNS agree extremely well (Fig. 3b, p. 416, in Ref. [6]). Therefore, results are here compared directly at $F = 22 \times 10^{-5}$ for which, however, no direct comparison with DNS is available. Figure 10b reports PSE results by Bertolotti et al. [6] (solid line) and the MS results computed with the present method (dashed line), showing a very good agreement, with a maximum error on the order of 1.5 %.

This discussion suggests the potential of multiple scales as a promising tool to improve transition prediction methods, including receptivity calculations and non-parallel effects. In fact, in addition to PSE, multiple scales provide the correct representation of an arbitrary initial condition, a more satisfactory theory, and a simpler numerical implementation (no numerical stability problems).

9 Comparison with three-dimensional results

In this section we compare our results, with or without non-parallel flow corrections, with those obtained by Crouch [22] who studied the receptivity of a three-dimensional boundary layer to cross-flow vortices in the parallel-flow framework. We consider the incompressible three-dimensional boundary-layer flow over an infinite swept wing modeled using the two-parameter family of similarity solutions for yawed wedge flows given by Cooke [18]. The first parameter, m, describes the intensity of the pressure gradient, whereas the second, Λ, is the sweep angle. The Hartree parameter $\beta_H = 2m/(1+m)$, associated with a wedge angle of $\beta_H\pi/2$, can be used instead of m. Following [22], we consider the reference frame $x^*y^*x^*$ such that x^* is the chordwise coordinate (normal to the leading edge), y^* is normal to the wing (pointing upwards) and z^* is the spanwise coordinate (parallel to the leading edge). The reference frame is set at a certain distance x_0^* from the leading edge. If Q_c denotes a constant free-stream velocity, then its components normal and parallel to the leading edge are, respectively,

$$U_c = Q_c \cos \Lambda \quad \text{and} \quad W_c = Q_c \sin \Lambda.$$

We introduce a reference length c^* such that the global Reynolds number is $R_c = \sqrt{(Q_c c^*)/\nu}$. All velocities are normalized with Q_e and all lengths with

$$\delta_r = \sqrt{\frac{\nu(x_0^* + x^*)}{U_e}},$$

where $U_e = U_c X^m$ is the chordwise velocity component at the edge of the boundary layer and $X = (x_0^* + x^*)/c^*$ is the normalized distance from the leading edge. If W_e denotes the constant velocity component parallel to z^* at the edge of the boundary layer,

$W_e = W_c$, then the total edge velocity Q_e is

$$Q_e(X) = \sqrt{U_e^2(X) + W_e^2}$$
$$= Q_c \cos \Lambda \sqrt{X^{2m} + \tan^2 \Lambda}.$$

We introduce the normalized normal-wall coordinate

$$y = \frac{y^*}{\delta_r} = y^* \sqrt{\frac{U_e}{\nu(x_0^* + x^*)}}$$

such that the three boundary-layer velocities components normalized with $Q_e(X)$ are

$$U(X, y) = \frac{U_e(X)}{Q_e(X)} f'(y)$$

$$V(X, y) = \frac{U_e(X)}{Q_e(X)} \frac{1-m}{2} \sqrt{\frac{\nu}{U_e(X)X}} \left[y f'(y) - \frac{m+1}{1-m} f(y) \right]$$

$$W(X, y) = \frac{W_e}{Q_e(X)} g(y),$$

where $f(y)$ and $g(y)$ are the Falkner-Skan-Cooke (FSC) family of profiles solutions of the two differential equations [18]

$$f''' + \frac{m+1}{2} f f'' + m(1 - f'^2) = 0 \tag{31}$$

$$g'' + \frac{m+1}{2} f g' = 0 \tag{32}$$

supplemented by the boundary conditions

$$f(0) = f'(0) = g(0) = 0 \quad \text{and} \quad f'(\infty) = g'(\infty) = 1.$$

Hereafter we focus on the same conditions used by Crouch [22]:

$$R_c = 1000, \qquad \Lambda = 30°, \qquad \beta_H = 0.6.$$

The dimensionless Navier-Stokes equation depend on the *local* Reynolds number

$$R = \frac{Q_e \delta_r}{\nu},$$

which is related to the *global* Reynolds number R_c by the equation

$$R = R_c^2 \frac{Q_e}{Q_c} \frac{X}{x_0 + x} = R_c^2 \frac{Q_e}{Q_c} \frac{\delta_r}{c^*}.$$

As opposed to the two-dimensional case, the surface perturbation depends on both x and z. If we assume a Fourier series expansion in z, then for a particular wavenumber β_n there is a corresponding receptivity coefficient (see its definition given by (29)) $\bar{r}_{h_n}(x)$. Crouch [22] observed that the conservation of phase imposes that the physical spanwise wavenumber

$$b = \beta_n \frac{R_c}{R} \frac{Q_e}{Q_c} = \beta_n \frac{1}{R_c} \frac{c^*}{\delta_r}$$

remains constant with changing chordwise position. Since

$$\frac{c^*}{\delta_r} = R_c \sqrt{\frac{\cos \Lambda}{X^{1-m}}},$$

the physical spanwise wavenumber reads

$$b = \beta_n \sqrt{\frac{\cos \Lambda}{X^{1-m}}}.$$

Here we focus on the coupling between an acoustic disturbance which is grazing the boundary layer in the chordwise direction with amplitude ϵQ_e,

$$\epsilon Q_e \big[(1 - \exp(-\sqrt{-i\omega_\epsilon R}\, y), 0, 0\big] \exp(-i\omega_\epsilon t),$$

where $\omega_\epsilon = \omega_{\text{TS}}$, and a disturbance of order δ originated by the wall roughness. The latter disturbance is obtained by employing the OS operator (see Sect. 6.3) with $\omega_\delta = 0$ and non-homogeneous boundary conditions stemming from the linearization at the wall. By recalling that the spanwise and wall-normal components of the acoustic perturbation are zero, the coupling of the disturbances at order $\epsilon\delta$ defined by equation (20) reduces to

$$\mathbf{y}_{\epsilon\delta} = - \begin{pmatrix} 0 \\ i\alpha_\delta u_\epsilon u_\delta + v_\delta (u_\epsilon)_y \\ i\alpha_\delta u_\epsilon v_\delta \\ i\alpha_\delta u_\epsilon w_\delta \end{pmatrix}, \tag{33}$$

where $\alpha_\delta = \alpha_{\text{TS}}$.

Figure 11a reproduces Fig. 6 of Ref. [22] and reports the amplitude ratio $A(X)/A(X_I)$ as a function of the chordwise position X, $A(X_I)$ being the amplitude of the resonant disturbance at the first neutral point. Parallel results obtained in the present work (solid line) match very well those of Ref. [22] (empty circles) whereas non-parallel results (dashed line) differ quite remarkably from the parallel ones for increasing chordwise position. This confirms the importance

(a) Amplitude ratio $A(X)/A(X_I)$

(b) Receptivity coefficient
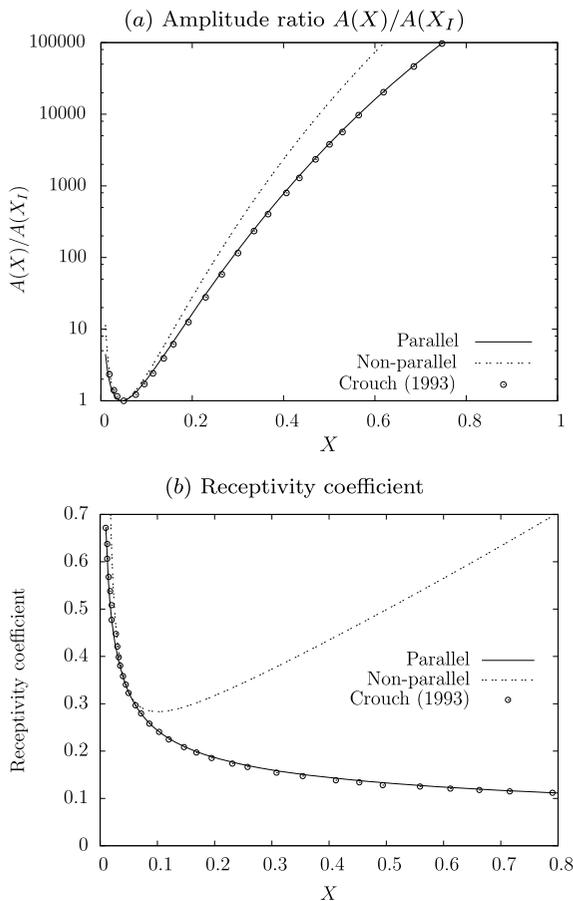
Fig. 11 Comparisons between parallel (*solid line*) and non-parallel (*dashed line*) results obtained in the present work and those reported in Ref. [22] obtained in the parallel framework, $F = \omega \nu / Q_c^2 = 3 \times 10^{-5}$ and $b = 0.45$. (**a**) Chordwise variation of the amplitude ratio $A(X)/A(X_I)$, $A(X_I)$ being the amplitude at the first neutral point. (**b**) Chordwise variation of the receptivity coefficient as defined in (29)

of including non-parallel corrections when considering cross-flow instabilities.

Figure 11b reproduces Fig. 9 of Ref. [22] and shows the chordwise variation of the receptivity coefficient as defined by (20). Parallel results (solid line) match again those of Ref. [22] (empty circles). When parallel corrections are introduced (dashed line), the receptivity coefficient increases quickly with the chordwise position and at $X = 0.8$ it becomes approximately 7 times larger than in the parallel case. This amplification is much greater than what was observed for the 2D boundary layer past a flat plate (see Fig. 4), where the maximum difference in the amplitude of the receptivity coefficient, when comparing

parallel and non-parallel cases, was on the order of only 10–15 %.

10 Summary and conclusions

Multiple scales are employed to account for non-parallel effects in the study boundary-layer receptivity to the quadratic mixing of environmental disturbances. This technique is introduced in its non-homogeneous formulation because of the intrinsically non-homogeneous nature of the receptivity problem.

Environmental disturbances are acoustic waves and vorticity waves, which travel in the free-stream, and wall vibration and wall roughness, which are localized at the wall. Since each of these disturbances alone cannot resonate with the TS wave, the resonant values of frequency and wavenumber are provided by the nonlinear mixing of at least two interacting disturbances. The receptivity coefficient, which relates the amplitude of the unstable wave to the physical amplitude of the disturbances from which it originated, is computed accounting for non-parallel flow effects and compared for different cases.

Results show that the acoustic wave and wall roughness perturbations can propagate deeply into the boundary layer, generating a forcing term that is mainly localized in the proximity of the wall and that leads to a quite large receptivity coefficient.

The vorticity wave interacting with wall roughness, on the contrary, provides a coupling that is confined mostly outside the boundary layer. This is caused by the asymptotic behavior of the streamwise and wall-normal velocity perturbations induced by the free-stream vorticity (they do not vanish at infinity). The forcing term originating from this interaction, which is one order of magnitude smaller than for the acoustic wave–wall roughness interaction, is therefore shifted far away from the wall and the dot product with the left eigenfunction, which reaches its maximum in the boundary layer, makes the receptivity coefficient smaller than in the previous case.

The acoustic and vorticity waves mixing shows a forcing that does not vanish far from the wall, but this is compensated by the left eigenfunction, which exponentially decay in y.

The interaction between a vibration of the wall (in the wall-normal direction) and wall roughness cannot lead to resonance with TS waves. This is proven by

the fact that the velocity disturbance at order $\epsilon\delta$ is the exact solution of the velocity perturbation induced by wall roughness on a wall vibrating in the normal direction.

By comparing the present approach with different approaches presented in previously published works to treat the flow non-parallelism, it is shown that multiple scales reproduce the results obtained with parabolized stability equations, but in addition they offer several advantages. The multiple-scale method does not suffer from numerical instability problems, is computationally inexpensive, its formulation is general, allows the correct representation of an arbitrary initial condition, and can be applied to any base flow obtained from computations or experimental data.

When the three-dimensional boundary layer over an infinite swept wing is considered, results show the important role played by the flow non-parallelism.

Appendix A: Homogeneous multiple-scale theory

Multiple scales are here briefly introduced in their homogeneous formulation, utilizing a simple one-dimensional example. Let

$$\boldsymbol{B}(t)\frac{d\mathbf{x}(t)}{dt} + \boldsymbol{C}(t)\mathbf{x}(t) = 0$$

be the evolution equation of a generic time-dependent linear system. If $\boldsymbol{B}$ is non singular, the previous expression can be written in a simpler form as

$$\frac{d\mathbf{x}(t)}{dt} = \boldsymbol{A}(t)\mathbf{x}(t) \tag{34}$$

where $\boldsymbol{A} = -\boldsymbol{B}^{-1}\boldsymbol{C}$. If the coefficient matrix $\boldsymbol{A}(t)$ is evaluated at a certain time $t = t_0$, the solution $\mathbf{x}(t)$ can be expressed as a function of the eigenvalues $\lambda_k(t_0)$ and right eigenvectors $\mathbf{u}_k(t_0)$,

$$\mathbf{x}(t) = \sum_{k=1}^{N} c_k \mathbf{u}_k(t_0) e^{\lambda_k(t_0)t}, \tag{35}$$

with N arbitrary coefficients c_k to be determined using the initial conditions. If the matrix $\boldsymbol{A}$ is not calculated at a certain time t_0 but varies in such a way that a long time (with respect to the typical characteristic time) is required in order to appreciate a variation of the eigenvalues λ_k and eigenvectors $\mathbf{u}_k$, then $\boldsymbol{A}$ is said to be slowly varying with t. In this case, a new time

scale $T = \tilde{\epsilon}t$ can be introduced so that an order-one variation of T occurs for a long variation of t, if $\tilde{\epsilon}$ is a small parameter that accounts for the slow dependence of $\boldsymbol{A}$ on t. With the substitution $T = \tilde{\epsilon}t$, equation (34) reads

$$\tilde{\epsilon}\frac{d\mathbf{x}(T)}{dT} = \boldsymbol{A}(T)\mathbf{x}(T) \tag{36}$$

and expression (35) becomes

$$\mathbf{x}(T) = \sum_{k=1}^{N} c_k \mathbf{u}_k(T_0) e^{\lambda_k(T_0)T/\tilde{\epsilon}}. \tag{37}$$

The asymptotic solution of (36), in the limit $\tilde{\epsilon} \to 0$, can be assumed to maintain the form (37), but with $\lambda_k(T)$ and $\mathbf{u}_k(T)$ replacing $\lambda_k(T_0)$ and $\mathbf{u}_k(T_0)$, and with c_k no more constant but depending on T and $\tilde{\epsilon}$, and expandable in power series of the parameter $\tilde{\epsilon}$. A single term in the summation (37) (the complete solution can be reconstructed by superimposition), in the case of a constant coefficient matrix $\boldsymbol{A} = \boldsymbol{A}(T_0)$, reads $\mathbf{x}(T) = \mathbf{u}_k(T_0)e^{\lambda_k(T_0)T/\tilde{\epsilon}}$. If the coefficient matrix $\boldsymbol{A}$ is slowing varying, the corresponding term can be written as $\mathbf{x}(T) = \mathbf{f}(T,\tilde{\epsilon})e^{\phi(T)/\tilde{\epsilon}}$ so that in the constant-coefficient case $\mathbf{f}(T,\tilde{\epsilon})$ and $\phi(T)$ respectively reduce to $\mathbf{f}(T,\tilde{\epsilon}) = \mathbf{u}_k(T_0)$ and $\phi(T) = \lambda_k(T_0)T$. We now assume that the vector $\mathbf{f}(T,\tilde{\epsilon})$ is expandable in power series of $\tilde{\epsilon}$ as

$$\mathbf{f}(T,\tilde{\epsilon}) = \sum_{n=0}^{\infty} \mathbf{f}_n(T)\tilde{\epsilon}^n,$$

which implies

$$\begin{aligned}
\mathbf{x}(T) &= \mathbf{f}(T,\tilde{\epsilon})e^{\phi(T)/\tilde{\epsilon}} \\
&= \big(\mathbf{f}_0(T) + \tilde{\epsilon}\mathbf{f}_1(T) + \tilde{\epsilon}^2\mathbf{f}_2(T) + \cdots\big)e^{\phi(T)/\tilde{\epsilon}}.
\end{aligned} \tag{38}$$

The term $\tilde{\epsilon}d\mathbf{x}/dT$ needed in (36) can now be computed from expression (38),

$$\begin{aligned}
&\tilde{\epsilon}\frac{d\mathbf{x}(T)}{dT} \\
&= \tilde{\epsilon}\bigg[\bigg(\frac{d\mathbf{f}_0(T)}{dT} + \tilde{\epsilon}\frac{d\mathbf{f}_1(T)}{dT} + \cdots\bigg)e^{\phi(T)/\tilde{\epsilon}} \\
&\quad + \frac{1}{\tilde{\epsilon}}\frac{d\phi(T)}{dT}\big(\mathbf{f}_0(T) + \tilde{\epsilon}\mathbf{f}_1(T) + \cdots\big)e^{\phi(T)/\tilde{\epsilon}}\bigg]
\end{aligned}$$

$$= \left[\frac{d\phi(T)}{dT} \mathbf{f}_0(T) + \tilde{\epsilon}\left(\frac{d\phi(T)}{dT} \mathbf{f}_1(T) + \frac{d\mathbf{f}_0(T)}{dT} \right) \right.$$
$$\left. + \mathcal{O}(\tilde{\epsilon}^2) \right] \mathrm{e}^{\phi(T)/\tilde{\epsilon}},$$

so that by introducing this derivative and the expansion (38) in the original system (36), collecting terms at different orders with respect to $\tilde{\epsilon}$, and dividing by the exponential factor, the following hierarchy of equations is found:

$$\frac{d\phi}{dT} \mathbf{f}_0(T) = A(T)\mathbf{f}_0(T)$$

$$\tilde{\epsilon}\left(\frac{d\phi}{dT} \mathbf{f}_1(T) + \frac{d\mathbf{f}_0}{dT} \right) = \tilde{\epsilon} A(T)\mathbf{f}_1(T)$$

$$\vdots = \vdots$$

$$\tilde{\epsilon}^n \left(\frac{d\phi}{dT} \mathbf{f}_n(T) + \frac{d\mathbf{f}_{n-1}}{dT} \right) = \tilde{\epsilon}^n A(T)\mathbf{f}_n.$$

The first equation reduces to the eigenvalue problem

$$\left[\frac{d\phi}{dT} I - A(T) \right] \mathbf{f}_0(T) = 0 \qquad (39)$$

and admits a non trivial solution if $d\phi/dT = \lambda_k(T)$. The solution $\mathbf{f}_0(T)$ is the right eigenvector but it is defined up to a multiplicative factor, because the normalization of $\mathbf{f}_0(T)$ is not unique, i.e. $\mathbf{f}_0(T) = c_k(T)\tilde{\mathbf{u}}_k(T)$, where the coefficient $c_k(T)$ is unknown and $\tilde{\mathbf{u}}_k(T)$ is the right eigenvector arbitrarily normalized.

The second equation, at order $\tilde{\epsilon}$, can be recast in the form

$$\left[\lambda_k(T) I - A(T) \right] \mathbf{f}_1(T) = \frac{d\mathbf{f}_0}{dT}, \qquad (40)$$

which is a singular problem since the coefficient matrix $[\lambda_k(T) I - A(T)]$ is the same as the one at order zero. The presence of a right-hand side term (RHS), however, requires the "compatibility condition" to be satisfied, i.e. the orthogonality between the RHS and the left eigenvector $\tilde{\mathbf{v}}_k(T)$ corresponding to the vanishing eigenvalue $\lambda_k(T)$,

$$\tilde{\mathbf{v}}_k(T) \cdot \frac{d\mathbf{f}_0}{dT} = 0. \qquad (41)$$

By expanding this condition and recalling that $\mathbf{f}_0(T) = c_k(T)\tilde{\mathbf{u}}_k(T)$, an equation for the unknown coefficient $c_k(T)$ is derived,

$$\tilde{\mathbf{v}}_k(T) \cdot \tilde{\mathbf{u}}_k(T) \frac{dc_k}{dT} + \tilde{\mathbf{v}}_k(T) \cdot \frac{d\tilde{\mathbf{u}}_k(T)}{dT} c_k = 0. \qquad (42)$$

Equation (42) is a first-order, homogeneous ordinary differential equation, for which a closed-form solution exists. Its solutions provides the coefficient $c_k(T)$ so that the product $c_k(T)\tilde{\mathbf{u}}_k(T) = \mathbf{f}_0(T)$ can eventually be computed. It is important to remark that the latter vector is unique, independently of the normalization, whereas the right eigenvector $\tilde{\mathbf{u}}_k(T)$ is not.

The same compatibility problem found at order $\tilde{\epsilon}$ is found also at next orders because the generic equation contains always the same singular matrix $[\lambda_k(T) I - A(T)]$. Conditions like (41) have thus to be imposed at each order. Once the equation for $\mathbf{f}_1(T)$ has been made compatible, the solution is still determined up to a factor that multiplies $\mathbf{u}_k(T)$ and that can be used to satisfy the compatibility condition at second order. The same procedure is repeated at each order.

In practical applications the solution is usually truncated at order zero, so that the state vector is $\mathbf{x}(T) = c_k(T)\tilde{\mathbf{u}}_k(T)\mathrm{e}^{\frac{\phi(T)}{\tilde{\epsilon}}} + \mathcal{O}(\tilde{\epsilon})$.

Appendix B: Details of the multiple-scale derivation for the Navier–Stokes equations

Given a small parameter $\tilde{\epsilon}$ that accounts for the slow variations in streamwise and spanwise directions, we introduce a new reference frame $x = \tilde{\epsilon}\hat{x}$, $y = \hat{y}$, $z = \tilde{\epsilon}\hat{z}$, $t = \hat{t}$ and rescale the base flow accordingly, $U(x, y, z) = \hat{U}(\hat{x}, \hat{y}, \hat{z})$, $V(x, y, z) = \hat{V}(\hat{x}, \hat{y}, \hat{z})/\tilde{\epsilon}$, $W(x, y, z) = \hat{W}(\hat{x}, \hat{y}, \hat{z})$. Because of the new scaling, the derivatives become $(\cdot)_{\hat{x}} = \tilde{\epsilon}(\cdot)_x$, $(\cdot)_{\hat{y}} = (\cdot)_y$, $(\cdot)_{\hat{z}} = \tilde{\epsilon}(\cdot)_z$, $(\cdot)_{\hat{t}} = (\cdot)_t$, and the derivatives of the base flow reduce to $\hat{U}_{\hat{x}} = \tilde{\epsilon}U_x$, $\hat{U}_{\hat{y}} = U_y$, $\hat{V}_{\hat{x}} = \tilde{\epsilon}^2 V_x$, $\hat{V}_{\hat{y}} = \tilde{\epsilon}V_y$, $\hat{W}_{\hat{x}} = \tilde{\epsilon}W_x$, and $\hat{W}_{\hat{y}} = W_y$. The general quantity $\hat{q}(\hat{x}, \hat{y}, \hat{z}, \hat{t})$ (which corresponds to $\hat{u}$, $\hat{v}$, $\hat{w}$ or $\hat{p}$ previously introduced) in the multiple-scale framework is expanded as

$$\hat{q}(\hat{x}, \hat{y}, \hat{z}, \hat{t})$$
$$= \left(q_0(x, y) + \tilde{\epsilon}q_1(x, y) + \cdots \right) \mathrm{e}^{\frac{i\theta(x)}{\tilde{\epsilon}} + i\beta z - i\omega t}, \quad (43)$$

where $q_0(x, y)$ and $q_1(x, y)$ are weak functions of the streamwise and wall-normal coordinates x and y, $\theta(x)$

is related to the streamwise wavenumber (which is a function of x), β is the spanwise wavenumber and ω the frequency. By introducing expansion (43) in the first derivatives expressed in the new reference frame, one obtains

$$(\hat{q})_{\hat{x}} = \tilde{\epsilon}\left((q_0)_x + \tilde{\epsilon}(q_1)_x + \cdots\right)e^{\frac{i\theta(x,z)}{\tilde{\epsilon}} - i\omega t}$$

$$+ \frac{i\alpha}{\tilde{\epsilon}}(q_0 + \tilde{\epsilon}q_1 + \cdots)e^{\frac{i\theta(x)}{\tilde{\epsilon}} + i\beta z - i\omega t}$$

$$= \tilde{\epsilon}\left(\frac{i\alpha}{\tilde{\epsilon}}q_0 + (q_0)_x + i\alpha q_1\right.$$

$$\left. + \tilde{\epsilon}(q_1)_x + \cdots\right)e^{\frac{i\theta(x)}{\tilde{\epsilon}} + i\beta z - i\omega t}$$

$$= \left(i\alpha q_0 + \tilde{\epsilon}(q_0)_x + \tilde{\epsilon}i\alpha q_1\right.$$

$$\left. + \tilde{\epsilon}^2(q_1)_x + \cdots\right)e^{\frac{i\theta(x)}{\tilde{\epsilon}} + i\beta z - i\omega t}$$

$$= \left[i\alpha q_0 + \tilde{\epsilon}\left[i\alpha q_1 + (q_0)_x\right]\right.$$

$$\left. + \mathcal{O}(\tilde{\epsilon}^2)\right]e^{\frac{i\theta(x)}{\tilde{\epsilon}} + i\beta z - i\omega t}$$

$$(\hat{q})_{\hat{y}} = \left[(q_0)_y + \tilde{\epsilon}(q_1)_y + \mathcal{O}(\tilde{\epsilon}^2)\right]e^{\frac{i\theta(x)}{\tilde{\epsilon}} + i\beta z - i\omega t}$$

$$(\hat{q})_{\hat{z}} = \left[i\beta q_0 + \tilde{\epsilon}i\beta q_1 + \mathcal{O}(\tilde{\epsilon}^2)\right]e^{\frac{i\theta(x)}{\tilde{\epsilon}} + i\beta z - i\omega t}$$

$$(\hat{q})_{\hat{t}} = -i\omega t\left[(q_0) + \tilde{\epsilon}(q_1) + \mathcal{O}(\tilde{\epsilon}^2)\right]e^{\frac{i\theta(x)}{\tilde{\epsilon}} + i\beta z - i\omega t},$$

where the streamwise wavenumber α is defined as $\alpha = \partial\theta/\partial x$. For the second derivatives, one gets

$$(\hat{q})_{\hat{x}\hat{x}} = \tilde{\epsilon}^2\left(-\frac{\alpha^2}{\tilde{\epsilon}^2} + \frac{2i\alpha}{\tilde{\epsilon}}(q_0)_x - \frac{\alpha^2}{\tilde{\epsilon}}q_1 + \frac{i\alpha_x}{\tilde{\epsilon}}q_0\right.$$

$$+ (q_0)_{xx} + 2i\alpha(q_1)_x + i\alpha_x q_1$$

$$\left. + \tilde{\epsilon}(q_1)_{xx} + \cdots\right)e^{\frac{i\theta(x)}{\tilde{\epsilon}} + i\beta z - i\omega t}$$

$$= \left[-\alpha^2 q_0 + \tilde{\epsilon}2i\alpha(q_0)_x - \tilde{\epsilon}\alpha^2 q_1 + \tilde{\epsilon}i\alpha_x q_0\right.$$

$$\left. + \mathcal{O}(\tilde{\epsilon}^2)\right]e^{\frac{i\theta(x)}{\tilde{\epsilon}} + i\beta z - i\omega t}$$

$$= \left[-\alpha^2 q_0 + \tilde{\epsilon}\left[-\alpha^2 q_1 + 2i\alpha(q_0)_x + i\alpha_x q_0\right]\right.$$

$$\left. + \mathcal{O}(\tilde{\epsilon}^2)\right]e^{\frac{i\theta(x)}{\tilde{\epsilon}} + i\beta z - i\omega t}$$

$$(\hat{q})_{\hat{y}\hat{y}} = \left[(q_0)_{yy} + \tilde{\epsilon}(q_1)_{yy} + \mathcal{O}(\tilde{\epsilon}^2)\right]e^{\frac{i\theta(x)}{\tilde{\epsilon}} + i\beta z - i\omega t}$$

$$(\hat{q})_{\hat{z}\hat{z}} = \left[-\beta^2 q_0 - \tilde{\epsilon}\beta^2 q_1 + \mathcal{O}(\tilde{\epsilon}^2)\right]e^{\frac{i\theta(x)}{\tilde{\epsilon}} + i\beta z - i\omega t},$$

so that the Laplacian in the new reference frame is

$$\nabla^2\hat{q} = \left[-(\alpha^2 + \beta^2)q_0 + (q_0)_{yy}\right.$$

$$+ \tilde{\epsilon}\left[-(\alpha^2 + \beta^2)q_0 + (q_0)_{yy} + 2i\alpha(q_0)_x\right.$$

$$\left. + i\alpha_x q_0\right] + \mathcal{O}(\tilde{\epsilon}^2)\right]e^{\frac{i\theta(x)}{\tilde{\epsilon}} + i\beta z - i\omega t}.$$

The base flow (U, V, W), the perturbations (u, v, w, p), the derivatives of the base flow and the derivatives of the perturbations are then introduced in the linearized Navier-Stokes equations (16) and boundary conditions (17), obtaining different systems of equations at different $\tilde{\epsilon}$-orders (19).

Matrices $\boldsymbol{A}$, $\boldsymbol{H}$ and $\boldsymbol{C}$ in equations (19) are respectively

$$\boldsymbol{A}(\alpha, \omega, R) = \begin{pmatrix} i\alpha & (\cdot)_y & i\beta & 0 \\ T & U_y & 0 & i\alpha \\ 0 & T & 0 & (\cdot)_y \\ 0 & W_y & T & i\beta \end{pmatrix}$$

$$\boldsymbol{H}(\alpha, R) = \begin{pmatrix} 1 & 0 & 0 & 0 \\ \bar{H} & 0 & 0 & 1 \\ 0 & \bar{H} & 0 & 0 \\ 0 & 0 & \bar{H} & 0 \end{pmatrix} = -i\frac{\partial\boldsymbol{A}}{\partial\alpha}$$

$$\boldsymbol{C}(\alpha, R) = \begin{pmatrix} 0 & 0 & 0 & 0 \\ C_1 & 0 & 0 & 0 \\ 0 & C_2 & 0 & 0 \\ W_x & 0 & C_2 & 0 \end{pmatrix}$$

where $\bar{H} = U - 2R^{-1}i\alpha$, $C_1 = U_x + V(\cdot)_y - R^{-1}i\alpha_x$, $C_2 = V_y + V(\cdot)_y - R^{-1}i\alpha_x$, $T = [i(\alpha U + \beta W - \omega) + R^{-1}(\alpha^2 + \beta^2 - (\cdot)_{yy})]$. Incidentally, matrix $\boldsymbol{A}$ is the well-known Orr–Sommerfeld operator.

Appendix C: Interaction between wall vibration and wall roughness

The perturbation originating from the interaction between wall vibration and wall roughness deserves a special remark because it can be proved that it does not result in a resonant wave. A structural rigid vibration of the wall may be of different forms; the surface can be finite or infinite and the vibration can be

parallel or normal to the wall. If an infinite surface is considered, the vibration parallel to the wall is a well-known problem with a closed-form solution (Stokes's second problem [58]) and is treated as the acoustic disturbance. Let us therefore concentrate on the problem of a rigid wall vibrating in the normal direction. If the wall is finite, a wall-normal vibration produces an induced flow in both parallel and normal directions with respect to the wall. The problem is thus decomposed into the known Stokes's second problem and the wall normal rigid-vibration problem (on an infinite surface).

The wall displacement is described by a function of time $y(t) = \epsilon e^{-i\omega_\epsilon t}$, where ϵ is the amplitude of the wall vibration and ω_ϵ is its frequency. It can be proved that the Navier–Stokes equations are invariant with respect to a coordinate transformation $Y = y - \epsilon e^{-i\omega_\epsilon t}$, which means that the solution in the reference frame moving with the wall is the solution obtained with the wall at rest and expressed as a function of $y - \epsilon e^{-i\omega_\epsilon t}$ rather than as a function of y. In order to prove it, we introduce a new reference frame $X = x$, $Y = y - \epsilon e^{-i\omega_\epsilon t}$, $Z = z$, $T = t$, so that the new unknowns are $U = u$, $V = v + \epsilon i\omega_\epsilon e^{-i\omega_\epsilon t}$, $W = w$, $P = p$, and the derivatives, as a function of the variables in the new reference frame, read $(\cdot)_t = (\cdot)_T + \epsilon i\omega_\epsilon e^{-i\omega_\epsilon t}$, $(\cdot)_x = (\cdot)_X, (\cdot)_y = (\cdot)_Y, (\cdot)_z = (\cdot)_Z$. By substituting these expressions in the Navier–Stokes equations, one gets:

$$U_X + V_Y + W_Z = 0$$

$$U_T + \epsilon i\omega_\epsilon e^{-i\omega_\epsilon T} U_Y + U U_X$$
$$\quad + \left(V - \epsilon i\omega_\epsilon e^{-i\omega_\epsilon T}\right) U_Y + W U_Z$$
$$\quad = -P_X + R^{-1}(U_{xx} + U_{yy} + U_{zz})$$

$$V_T + \epsilon i\omega_\epsilon e^{-i\omega_\epsilon T} V_Y + U V_X + \left(V - \epsilon i\omega_\epsilon e^{-i\omega_\epsilon T}\right)$$
$$\quad \times V_Y + W V_Z$$
$$\quad = -P_Y + R^{-1}(V_{xx} + V_{yy} + V_{zz})$$

$$W_T + \epsilon i\omega_\epsilon e^{-i\omega_\epsilon T} W_Y + U W_X$$
$$\quad + \left(V - \epsilon i\omega_\epsilon e^{-i\omega_\epsilon T}\right) W_Y + W W_z$$
$$\quad = -P_z + R^{-1}(W_{xx} + W_{yy} + W_{zz}).$$

These equations can be simplified as

$$U_X + V_Y + W_Z = 0$$

$$U_T + U U_X + V U_Y + W U_Z$$
$$\quad = -P_X + R^{-1}(U_{xx} + U_{yy} + U_{zz})$$

$$V_T + U V_X + V V_Y + W V_Z$$
$$\quad = -P_Y + R^{-1}(V_{xx} + V_{yy} + V_{zz}$$

$$W_T + U W_X + V W_Y + W W_z$$
$$\quad = -P_z + R^{-1}(W_{xx} + W_{yy} + W_{zz}),$$

which are the incompressible Navier–Stokes equations in the common form.

Let us now go back to the original transformation $Y = y - \epsilon e^{-i\omega_\epsilon t}$. Since the quantity $\epsilon e^{-i\omega_\epsilon t}$ is very small, it is possible to linearize the solution $\mathbf{v}(x, y - \epsilon e^{-i\omega_\epsilon t}, z)$ about y via a Taylor expansion:

$$\mathbf{v}\left(x, y - \epsilon e^{-i\omega_\epsilon t}, z\right)$$
$$\quad = \mathbf{v}(x, y, z) - \epsilon \mathbf{v}_y(y) e^{-i\omega_\epsilon t} + \mathcal{O}(\epsilon^2). \quad (44)$$

When wall roughness is introduced on a wall at rest, the solution is in the form

$$\mathbf{v}(x, y, z) = \mathbf{V}(x, y, z) + \delta\mathbf{v}_\delta(x, y, z) + \mathcal{O}(\delta^2), \quad (45)$$

where $\mathbf{V}$ is the base flow and $\mathbf{v}_\delta$ is the disturbance velocity induced by wall roughness. If the effects of wall roughness and wall vibration are coupled, the equations can be written in the reference frame $y - \epsilon e^{-i\omega_\epsilon t}$. By doing so, and substituting expression (45) in the Taylor expansion (44), one gets

$$\mathbf{v}\left(x, y - \epsilon e^{-i\omega_\epsilon t}, z\right)$$
$$\quad = \mathbf{V}(x, y, z) - \epsilon \mathbf{V}_y(x, y, z) e^{-i\omega_\epsilon t} + \delta\mathbf{v}_\delta(x, y, z)$$
$$\quad - \epsilon\delta \frac{\partial \mathbf{v}_\delta(x, y, z)}{\partial y} e^{-i\omega_\epsilon t} + \mathcal{O}(\epsilon^2) + \mathcal{O}(\delta^2). \quad (46)$$

Expression (46) can now be compared with the velocity decomposition (2), carried out in Sect. 3. In the case of wall roughness – wall vibration interaction, $\omega_\delta = 0$ (the disturbance due to wall roughness is stationary) so that equation (2) reduces to

$$\mathbf{v}(x, y, z) = \mathbf{V}(x, y, z) + \epsilon\mathbf{v}_\epsilon(x, y, z) e^{-i\omega_\epsilon t}$$
$$\quad + \delta\mathbf{v}_\delta(x, y, z) + \epsilon\delta\mathbf{v}_{\epsilon\delta}(x, y, z) e^{-i\omega_\epsilon t}$$
$$\quad + \mathcal{O}(\epsilon^2) + \mathcal{O}(\delta^2). \quad (47)$$

By comparing terms at order ϵ and $\epsilon\delta$ in equations (46) and (47) it is clear that

$$\mathbf{v}_\epsilon(x, y, z) = -\frac{\partial \mathbf{V}(x, y, z)}{\partial y}$$

$$\mathbf{v}_{\epsilon\delta}(x, y, z) = -\frac{\partial \mathbf{v}_\delta(x, y, z)}{\partial y}. \tag{48}$$

Therefore, the velocity disturbance at order $\epsilon\delta$ is not originating from the interaction between the two disturbances at order ϵ and δ but is the exact solution of the velocity perturbation induced by wall roughness on a wall vibrating in the normal direction.

References

1. Airiau C (2000) Non-parallel acoustic receptivity of a Blasius boundary layer using an adjoint approach. Flow Turbul Combust 65(3/4):347–367
2. Asai M, Aiba K, Nishioka M (1996) A nonlinearity-coupled receptivity process generating a Tollmien–Schlichting wave behind a backward-facing step. Fluid Dyn Res 17:225–236
3. Ashpis AE, Reshotko E (1990) The vibrating ribbon problem revisited. J Fluid Mech 213:531–547
4. Bender CM, Orszag SA (1978) Advanced mathematical methods for scientists and engineers. McGraw–Hill, New York
5. Bertolotti FP (2000) Receptivity of three-dimensional boundary-layers to localized wall roughness and suction. Phys Fluids 12(7):1799–1809
6. Bertolotti FP, Herbert T, Spalart PR (1992) Linear and non linear stability of the Blasius boundary layer. J Fluid Mech 242:441–474
7. Bodonyi RJ, Duck PW (1992) Boundary-layer receptivity due to a wall suction and control of Tollmien–Schlichting waves. Phys Fluids A 4(6):1206–1214
8. Bodonyi RJ, Welch WJC, Duck PW, Tadjfar M (1989) A numerical study of the interaction between unsteady free-stream disturbances and localized variations in surface geometry. J Fluid Mech 209:285–308
9. Bouthier M (1972) Stabilité linéaire des écoulements presque parallélles. J Méch 11:599–621
10. Casalis G, Gouttenoire C, Troff B (1997) Etude de recéptivité de bord d'attaque et de recéptivité localisée par simulation numérique directe. In: First AFOSR international conference on DNS and LES, Ruston, LA (USA), pp 4–8
11. Casalis G, Gouttenoire C, Troff B (1997) Recéptivité localisée de la coche limite. C R Acad Sci Paris 325:571–576
12. Chiu WK, Norton MP (1990) The receptivity of laminar boundary layer to leading edge vibration. J Sound Vib 141:143–173
13. Chiu WK, Soria J, Norton MP (1995) Laminal boundary layer receptivity to transverse structural vibration. J Sound Vib 186(3):463–493
14. Choudhari M (1994) Distributed acoustic receptivity in laminar flow control configurations. Phys Fluids 6(2):489–506
15. Choudhari M, Kerschen E (1990) Boundary layer receptivity due to three dimensional convected gust. In: Instability and transition workshop (ICASE/NASA LaRC). Springer, Berlin
16. Choudhari M, Kerschen E (1990) Instability wave patterns generated by interaction of sound waves with three-dimensional wall suction or roughness. AIAA paper 90-0119
17. Choudhari M, Streett CL (1992) A finite Reynolds-number approach for the prediction of boundary-layer receptivity in localized regions. Phys Fluids A 4(11):2495–2514
18. Cooke JC (1950) The boundary layer of a class of infinite yawed cylinders. Proc Camb Philol Soc 46:645–648
19. Crouch JD (1992) Localized receptivity of boundary layers. Phys Fluids A 4(7):1408–1414
20. Crouch JD (1992) Non-localized receptivity of boundary layers. J Fluid Mech 244:567–581
21. Crouch JD (1993) Receptivity and the evolution of boundary-layer instabilities over short-scale waviness. Phys Fluids A 5(3):561–567
22. Crouch JD (1993) Receptivity of three-dimensional boundary layers. AIAA paper 93-0074
23. Crouch JD (1994) Distributed excitation of Tollmien–Schlichting waves by vortical fre-stream disturbances. Phys Fluids 6(1):217–223
24. Crouch JD, Spalart PR (1995) A study of non-parallel and nonlinear effects on the localized receptivity of the boundary layers. J Fluid Mech 290:29–37
25. Dietz AJ (1999) Local boundary-layer receptivity to a convected free-stream disturbances. J Fluid Mech 378:291–317
26. Duck PW, Ruban AI, Zhikharev CN (1996) The generation of Tollmien–Schlichting waves by free-stream turbulence. J Fluid Mech 312:341–371
27. Gaster M (1965) On the generation of spatially growing waves in a boundary layer. J Fluid Mech 22:433–441
28. Gaster M (1974) On the effects of boundary-layer growth on flow stability. J Fluid Mech 66:465–480
29. Gaster M, Sengupta TK (1993) The generation of disturbance in a boundary layer by wall perturbations: the vibrating ribbon revisited once more. In: Instability and turbulence in engineering flows. Springer, Berlin, pp 31–49
30. Goldstein ME (1983) The evolution of Tollmien–Schlichting waves near a leading edge. J Fluid Mech 127:59–81
31. Goldstein ME (1985) Scattering of acoustic wave into Tollmien–Schlichting waves by small streamwise variation in surface geometry. J Fluid Mech 154:509–529
32. Goldstein ME, Hultgren LS (1987) A note on the generation of Tollmien–Schlichting waves by sudden surface curvature change. J Fluid Mech 181:519–525
33. Goldstein ME, Hultgren LS (1989) Boundary-layer receptivity to long-wave free-stream disturbances. Annu Rev Fluid Mech 21:137–166
34. Goldstein ME, Leib SJ, Cowel SJ (1987) Generation of Tollmien–Schlichting waves on interactive marginally separated flows. J Fluid Mech 181:485–517
35. Herbert T (1997) Parabolized stability equations. Annu Rev Fluid Mech 29:245–283
36. Hill DC (1995) Adjoint systems and their role in the receptivity problem for boundary layers. J Fluid Mech 292:183–204

37. Hunt JCR, Durbin PA (1999) Perturbed vortical layers and shear sheltering. Fluid Dyn Res 24:375–404

38. Kachanov YS (2000) Three-dimensional receptivity of boundary layers. Eur J Mech B, Fluids 19:723–744

39. Kachanov YS, Kozlov VV, Levchenko VY (1979) Occurrence of Tollmien–Schlichting waves in the boundary layer under the effect of external perturbations. Fluid Dyn Res 13:704–711

40. Kerimbekov RM, Ruban AI (2005) Receptivity of boundary layers to distributed wall vibrations. Philos Trans R Soc Lond Ser A, Math Phys Sci 363:1145–1155

41. Kerschen E (1989) Boundary layer receptivity. AIAA paper 90-1109

42. Kerschen E (1991) Linear and nonlinear receptivity to vortical free stream disturbances. ASME-FED 114

43. Kobayashi R, Fukunishi Y, Nishikawa T, Kato T (1994) The receptivity of flat plate boundary layers with two-dimensional roughness elements to free-stream sound and its control. In: Proceeding of the IUTAM symposium on laminar–turbulent transition, Sendai, Japan

44. Luchini P, Bottaro A (1998) Gørtler vortices: a backward-in-time approach to the receptivity problem. J Fluid Mech 363:1–23

45. De Matteis P, Donelli RS, Luchini P (1995) Application of the ray-tracing theory to the stability analysis of three-dimensional incompressible boundary layers. In: Atti del XIII congresso nazionale AIDAA, Roma, 11–15 Sett, vol 1, pp 1–10

46. Michalke A (1995) Receptivity of axisymmetric boundary layers due to excitation by a Dirac point source at the wall. Eur J Mech B, Fluids 14(4):373–393

47. Michalke A (1997) Excitation of a 3D-wavetrain by Dirac point source at the wall and its growth in a decelerating laminar boundary layer. Eur J Mech B, Fluids 16(6):779–795

48. Michalke A, Neemann K (1997) Excitation of instability waves in wall boundary layers with adverse pressure gradients by various types of Dirac sources. Acta Mech 122:33–48

49. Morkovin MV (1969) On the many faces of transition. In: Wells CD (ed) Viscous drag reduction. Plenum, New York, pp 1–31

50. Nayfeh AH, Ashour ON (1994) Acoustic receptivity of a boundary layer to Tollmien–Schlichting waves resulting from a finite-heigh hump at finite Reynolds numbers. Phys Fluids 6(11):3705–3716

51. Pralits JO, Hanifi A, Henningson DH (2002) Adjoint-based optimization of steady suction for disturbance control in incompressible flows. J Fluid Mech 467:129–161

52. Reshotko E (1976) Boundary-layer stability and transition. Annu Rev Fluid Mech 8:311–349

53. Ruban AI (1985) On generation of Tollmien–Schlichting waves by sound. Fluid Dyn 19:709–716

54. Ryzhov OS, Terent'ev ED (1986) On the transition mode characterizing the triggering of a vibrator in the subsonic boundary layer on a plate. Prikl Mat Meh 50(6):974–986. (English translation: J. Appl. Math. Mech. 50(6):753–762)

55. Saric WS, Hoos J, Radeztsky R (1991) Boundary-layer receptivity of sound with roughness. In: Reda DC, Reed HL, Kobayshi R (eds) Boundary layer stability and transition to turbulence. American Society of Mechanical Engineers, New York

56. Saric WS, Nayfeh AH (1975) Nonparallel stability of boundary-layer flows. Phys Fluids 18(8):945–950

57. Saric WS, Reed HL, Kerschen EJ (2000) Boundary-layer receptivity to freestream disturbances. Annu Rev Fluid Mech 34:291–319

58. Schlichting H (1979) Boundary-layer theory, 7th edn. McGraw–Hill, New York

59. Schubauer GB, Skramstad HK (1948) Laminar-boundary-layer oscillations and transition on a flat plate. NACA TR-909

60. Sengupta TK, Ballav M, Hijhawan S (1994) Generation of Tollmien–Schlichting waves by harmonic excitation. Phys Fluids 6(3):1213–1222

61. Tadjfar M, Bodonyi RJ (1992) Receptivity of a laminar boundary layer to the interaction of a three-dimensional roughness element with time harmonic free-stream disturbances. J Fluid Mech 242:701–720

62. Terent'ev ED (1981) The linear problem of a vibrator in a subsonic boundary layer. Prikl Mat Meh 45(6):1049–1055. (English translation: J. Appl. Math. Mech. 45(6):791–795)

63. Terent'ev ED (1984) The linear problem of a vibrator performing harmonic oscillations at supercritical frequencies in a subsonic boundary layer. Prikl Mat Meh 48(2):264–272. (English translation: J. Appl. Math. Mech. 48(2):184–191)

64. Whitham GB (1999) Linear and nonlinear waves. Wiley, New York

65. Wu X (1999) Generation of Tollmien–Schlichting waves by convecting gusts interacting with sound. J Fluid Mech 397:285–316

66. Wu X (2001) On local boundary-layer receptivity to vortical disturbances in the free stream. J Fluid Mech 449:373–393

67. Wu X (2001) Receptivity of boundary layers with distributed roughness to vortical and acoustic disturbances: a second-order asymptotic theory and comparison with experiments. J Fluid Mech 431:91–133

68. Zhigulev VN, Fedorov AV (1987) Boundary layer receptivity to acoustic disturbances. J Appl Mech Tech Phys 28(1):28–35

69. Zhigulev VN, Tumin AM (1987) Origin of turbulence. Nauka, Novosibirsk

70. Zuccher S (2001) Receptivity and control of flow instabilities in a boundary layer. PhD dissertation, Politecnico di Milano